Global Change Biology WILEY

RESEARCH ARTICLE

Methane in West Siberia terrestrial seeps: Origin, transport, and metabolic pathways of production

Aleksandr F. Sabrekov[1,2] | Irina E. Terentieva[3] | Gregory J. McDermid[3] |
Yuriy V. Litti[4] | Anatoly S. Prokushkin[5] | Mikhail V. Glagolev[1,6] |
Alexey V. Petrozhitskiy[7,8] | Peter N. Kalinkin[9] | Dmitry V. Kuleshov[8,10] |
Ekaterina V. Parkhomchuk[8,10]

[1]UNESCO Department "Environmental Dynamics and Global Climate Changes", Ugra State University, Khanty-Mansiysk, Russia

[2]V.N. Sukachev Laboratory of Biogeocenology, A.N. Severtsov Institute of Ecology and Evolution, Russian Academy of Sciences, Moscow, Russia

[3]Department of Geography, University of Calgary, Calgary, Canada

[4]Laboratory of Microbiology of Anthropogenic Habitats, Winogradsky Institute of Microbiology, Research Center of Biotechnology of the Russian Academy of Sciences, Moscow, Russia

[5]Laboratory of Biogeochemical Cycles in Forest Ecosystems, VN Sukachev Institute of Forest SB RAS, Krasnoyarsk, Russia

[6]Department of Physics and Reclamation, Faculty of Soil Science, Lomonosov Moscow State University, Moscow, Russia

[7]Laboratory 5-2, Budker Institute of Nuclear Physics SB RAS, Novosibirsk, Russia

[8]AMS Golden Valley, Novosibirsk State University, Novosibirsk, Russia

[9]The Group of Template Synthesis, Boreskov Institute of Catalysis SB RAS, Novosibirsk, Russia

[10]Laboratory Alsotope, Institute of Archaeology and Ethnography SB RAS, Novosibirsk, Russia

Correspondence
Aleksandr F. Sabrekov, UNESCO Department "Environmental Dynamics and Global Climate Changes", Ugra State University, Khanty-Mansiysk, Russia.
Email: sabrekovaf@gmail.com

Abstract

The expansive plains of West Siberia contain globally significant carbon stocks, with Earth's most extensive peatland complex overlying the world's largest-known hydrocarbon basin. Numerous terrestrial methane seeps have recently been discovered on this landscape, located along the floodplains of the Ob and Irtysh Rivers in hotspots covering more than $2500\,km^2$. We articulated three hypotheses to explain the origin and migration pathways of methane within these seeps: (H1) uplift of Cretaceous-aged methane from deep petroleum reservoirs along faults and fractures, (H2) release of Oligocene-aged methane capped or trapped by degrading permafrost, and (H3) horizontal migration of Holocene-aged methane from surrounding peatlands. We tested these hypotheses using a range of geochemical tools on gas and water samples extracted from seeps, peatlands, and aquifers across the $120,000\,km^2$ study area. Seep-gas composition, radiocarbon age, and stable isotope fingerprints favor the peatland hypothesis of seep-methane origin (H3). Organic matter in raised bogs is the primary source of seep methane, but observed variability in stable isotope composition and concentration suggest production in two divergent biogeochemical settings that support distinct metabolic pathways of methanogenesis. Comparison of these parameters in raised bogs and seeps indicates that the first is bogs, via CO_2 reduction methanogenesis. The second setting is likely groundwater, where dissolved organic carbon from bogs is degraded via chemolithotrophic acetogenesis followed

by acetate fermentation methanogenesis. Our findings highlight the importance of methane lateral migration in West Siberia's bog-dominated landscapes via intimate groundwater connections. The same phenomenon could occur in similar landscapes across the boreal-taiga biome, thereby making groundwater-fed rivers and springs potent methane sources.

1 | INTRODUCTION

Methane (CH_4) is the planet's second-most important anthropogenic greenhouse gas (Canadell et al., 2021), with a global warming potential 27–30 times higher than CO_2 on a 100-year time horizon (Forster et al., 2021). Earth's terrestrial hydrocarbon degassing (onshore seepage) contributes an estimated 20–50 $TgCH_4$ to annual global emissions, second only to wetlands and freshwater ecosystems among natural sources (Canadell et al., 2021; Etiope et al., 2019; Saunois et al., 2020). Seep methane biogeochemistry is complex and multivariate, involving different origin and production pathways (Milkov & Etiope, 2018; Walter Anthony et al., 2012; Whiticar, 1999). Primary microbial methane is produced by *Archaea* microorganisms (methanogens) in the terminal step of the anaerobic organic matter degradation in surface soils and sediments (Conrad, 2020; Whiticar, 1999). Methanogens primarily use two distinct metabolic mechanisms for methane production: acetate fermentation and CO_2 reduction (Conrad, 2005, 2020). In contrast, thermogenic methane is generated during thermal cracking of organic matter, including petroleum, without microbial activity (Etiope, 2015; Milkov & Etiope, 2018; Whiticar, 1999). Finally, secondary microbial methane has been acknowledged as a meaningful methane pool (Milkov, 2010). This methane is produced in the final step of the anaerobic petroleum biodegradation, which is catalyzed by methanogens, inhabiting subsurface sediments (Milkov, 2018; Milkov & Etiope, 2018).

Understanding the origin, pathways of production, and transport mechanisms of methane from regional terrestrial seeps is a matter of both practical and academic interest. For example, seep-mapping exercises in regions where methane is sourced from underlying oil and gas reservoirs could assist with operational petroleum exploration (Schumacher, 2010). Knowing the source of methane from local terrestrial seeps also helps scientists appraise the size of regional methane pools. Such knowledge is critical for predicting how climate change will affect global methane budgets (Conrad, 2020; Etiope et al., 2019). For example, emission of thermogenic and secondary microbial methane is likely to decrease for depleted oil and gas reservoirs (Etiope, 2015). A better understanding of transportation mechanisms between sources and seeps could also help researchers identify new CH_4 emission hot spots worldwide (Ciotoli et al., 2020).

Recent studies have reported the discovery of a terrestrial methane seeps in the geographical center of the West Siberia Lowlands,

near the confluence of Ob and Irtysh Rivers (Belova et al., 2013; Oshkin et al., 2014). These seeps occur as groups of small craters and funnels with gas ebullition and groundwater discharge (Figure 1). The seeps represent hot spots of methane emissions, with CH_4 fluxes reaching hundreds of $mgCH_4\ h^{-1}$ per seep (Belova et al., 2013; Oshkin et al., 2014). Methane-rich seeps have been observed throughout the surrounding region, particularly along broad stretches of the Ob (middle reach) and Irtysh (lower reach) River floodplains (Danilova et al., 2021; Terentieva et al., 2022). Working with satellite imagery, Terentieva et al. (2022) mapped 2885 km^2 of seep zones in the region.

The source and metabolic pathways of methane in the Ob and Irtysh River seeps are not yet fully understood. Oshkin et al. (2014) suggested that the methane is primary microbial in origin. The authors based this suggestion on the stable carbon isotope ratio in methane samples ($\delta^{13}C(CH_4)$), which fell in the range of −71.1 to −71.3‰. However, the reported values could also be attributed to thermogenic methane from low-maturity source rocks, as well as to secondary microbial methane (Milkov & Etiope, 2018). Since a variety of sources can produce methane with similar $\delta^{13}C(CH_4)$ signatures, multiple indicators are needed to identify methane origin of these seeps with confidence (Etiope, 2015). In addition, Oshkin et al.'s (2014) observations were obtained from a single site: a remote research station called Mukhrino, located 20 km south of the confluence of the Ob and Irtysh Rivers. Since methane in seeps of the same region can have different origins (Walter Anthony et al., 2012), spatially resolved sampling is necessary to obtain reliable conclusions on seep methane biogeochemistry.

There are three hypotheses to explain the origin and migration pathways of methane seeps along the Ob and Irtysh River floodplains (Figure 2).

1.1 | H1. Methane uplift from oil and gas reservoirs

The West Siberian Basin, which overlaps geographically with the West Siberia Lowlands, is the largest known hydrocarbon reservoir in the world with more than 30,000 Pg of proven methane deposits (Khafizov et al., 2022). Oil and gas reservoirs are located in late-Jurassic and Cretaceous deposits, between 0.6 and 3 km below the surface (Khafizov et al., 2022; Milkov, 2010). According to this hypothesis, methane from source deposits migrates to the upper layers through
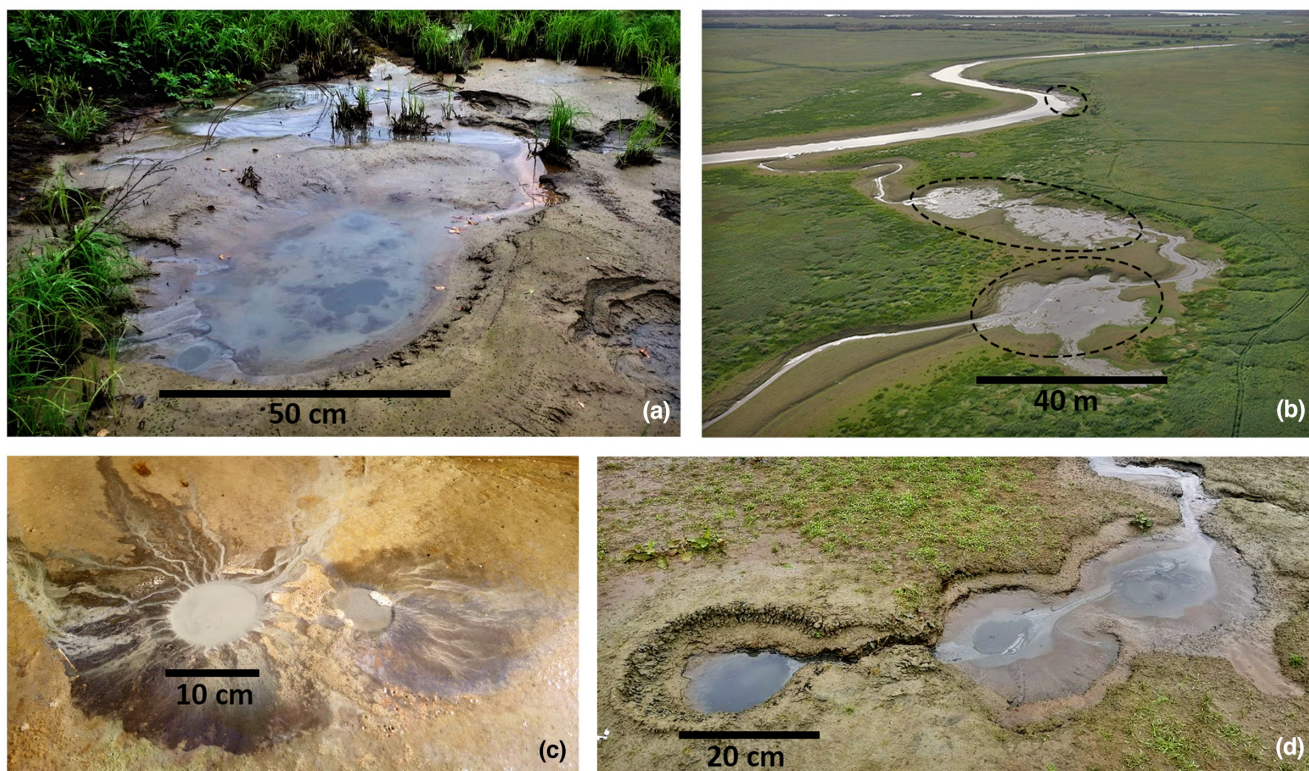
FIGURE 1 Field photos illustrate different morphologies of methane seeps along the Ob River floodplain in Western Siberia: (a) bubbling pool, (b) flooded areas in the stream channel, (c) non-flooded crater-like structures, and (d) a chain of funnels forming small creek due to groundwater discharge.

faults and fractures in impermeable cap deposits, then discharges with groundwater on the surface. This methane should be ancient (>60 million years) and is either of thermogenic or secondary microbial origin.

1.2 | H2. Degradation of relict permafrost

Within the study region, relict permafrost is located at depths of 100–300 m in an Oligocene confined aquifer under a thin (10–20 m) layer of clay (Brown et al., 1997). According to this hypothesis, ancient (>27 million years) primary microbial methane from degrading relict permafrost dissolves into surrounding groundwater and either percolates into the upper Quaternary aquifer or directly discharges as artesian springs at the surface. Similar processes have been observed in Alaska, where climate-induced degradation of permafrost has increased emission of both biogenic and thermogenic methane (Walter Anthony et al., 2012). Large amounts of methane could be trapped in permafrost by cryogenic displacement (Kraev et al., 2017), including West-Siberian permafrost (Kraev et al., 2019).

1.3 | H3. Horizontal transport of methane from raised bogs through groundwater

According to this hypothesis, modern (<12,000 years) primary microbial methane is transported by horizontal groundwater flow

and discharged on the floodplains. About third of the West Siberia Lowlands is covered by raised bogs (Kremenetski et al., 2003; Sheng et al., 2004; Terentieva et al., 2016) with organic deposits up to 6 m deep (Turunen et al., 2001). Solutes can migrate downward from raised bog to groundwater through aquitard via either advection (Glaser et al., 2016; Levy et al., 2014; Reeve et al., 2009) or diffusion (Beer & Blodau, 2007; Clymo & Bryant, 2008; Shoemaker & Schrag, 2010). Raised bogs in the study region are typically underlain by illite–kaolinite aquitards several meters thick with very low hydraulic conductivity (Leschinsky et al., 2006). However, both dissolved organic carbon (DOC) and dissolved methane can pass through such diffusion-dominated aquitards on a timescale of several thousand years, as calculated using diffusion coefficients from Jacobs et al. (2013). DOC could be further degraded in groundwater under anaerobic conditions, fueling methanogenesis (Aravena et al., 2004). Since temperature, pH, and substrate concentrations and quality are different between raised bogs and groundwater, methanogenesis could proceed via distinct metabolic pathways in these biogeochemical settings (Conrad, 2020). The latter would result in variable C and H stable isotopes ratios in methane produced in these settings.

The primary motivation of the current work is to understand the origin and production pathways of methane from these widespread seeps, as well as their role in the regional methane cycle. To test the hypotheses suggested above, we used multiple biogeochemical tools including (i) light hydrocarbons composition; (ii) stable isotope
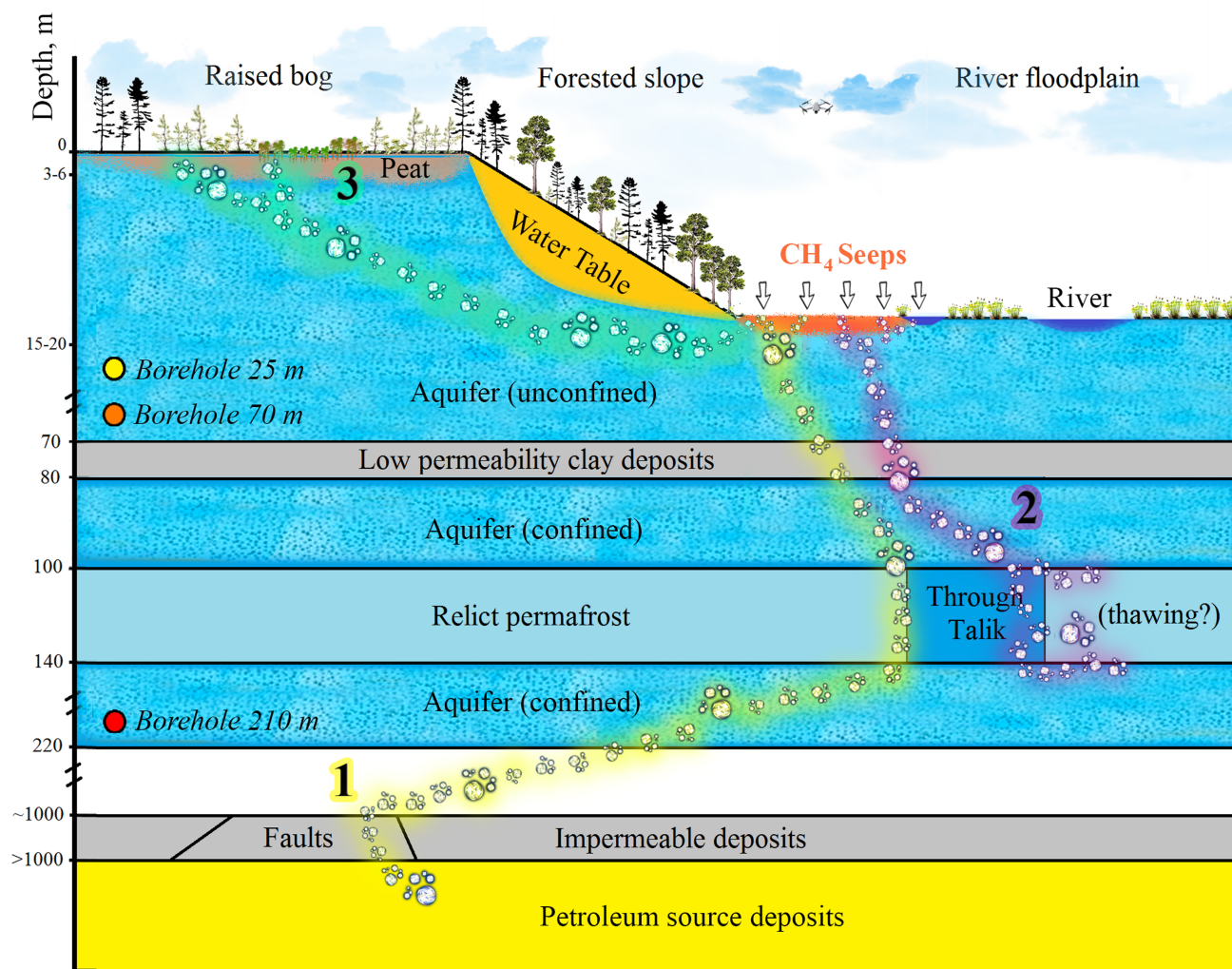
FIGURE 2 This graphic illustrates the three hypotheses of methane origin in West-Siberian methane seeps: (H1) methane uplift from oil and gas reservoirs; (H2) degradation of relict permafrost in Oligocene deposits; and (H3) horizontal transport of methane from raised bogs through ground waters in Quaternary deposits. All depths are given for Khanty-Mansiysk city according to Brown et al. (1997) and Milkov (2010).

composition of co-occurring methane, carbon dioxide and water; and (iii) radiocarbon content of methane. To obtain spatially representative data, we sampled gas and water from 50 sites with seeps across a 120,000 km² study area. In addition, we compared biogeochemical parameters of methane in seeps and its probable source to get insights into the mechanisms responsible for transporting methane from source to seeps and accompanying biogeochemical processes.

2 | MATERIALS AND METHODS

2.1 | Study region

The study region is in the boreal-taiga zone of the West Siberia Lowlands, spanning 400 km in an east–west direction and 300 km in a north–south direction (Figure 3). The region has a subarctic

climate (classified as Dfc according to the Köppen–Geiger system) with warm, short summers and long, cold winters. The average annual air temperature ranges from −3°C to +1°C, while mean annual precipitation ranges from 400 to 650 mm, based on data from 1981 to 2010 (www.pogodaiklimat.ru, accessed on April 5th, 2022). The highest precipitation, ranging from 150 to 250 mm, occurs during the summer months (Bulatov, 2007; Dyukarev et al., 2021). The region experiences a continuous snowpack, which lasts for more than 5 months and reaches depths of 40–80 cm. The soil in the region freezes to depths of 15–50 cm (Dyukarev et al., 2021). Snow melt typically occurs in April and May, resulting in seasonal floods that recede by the end of July. The region receives more precipitation than it experiences evapotranspiration, with the average surplus being 20–100 mm (Bulatov, 2007; Dyukarev et al., 2021). The topography of the region is relatively flat, with elevations ranging from 10 to 20 m above sea level in floodplains and 30–60 m in watersheds (Bulatov, 2007; Kremenetski et al., 2003).
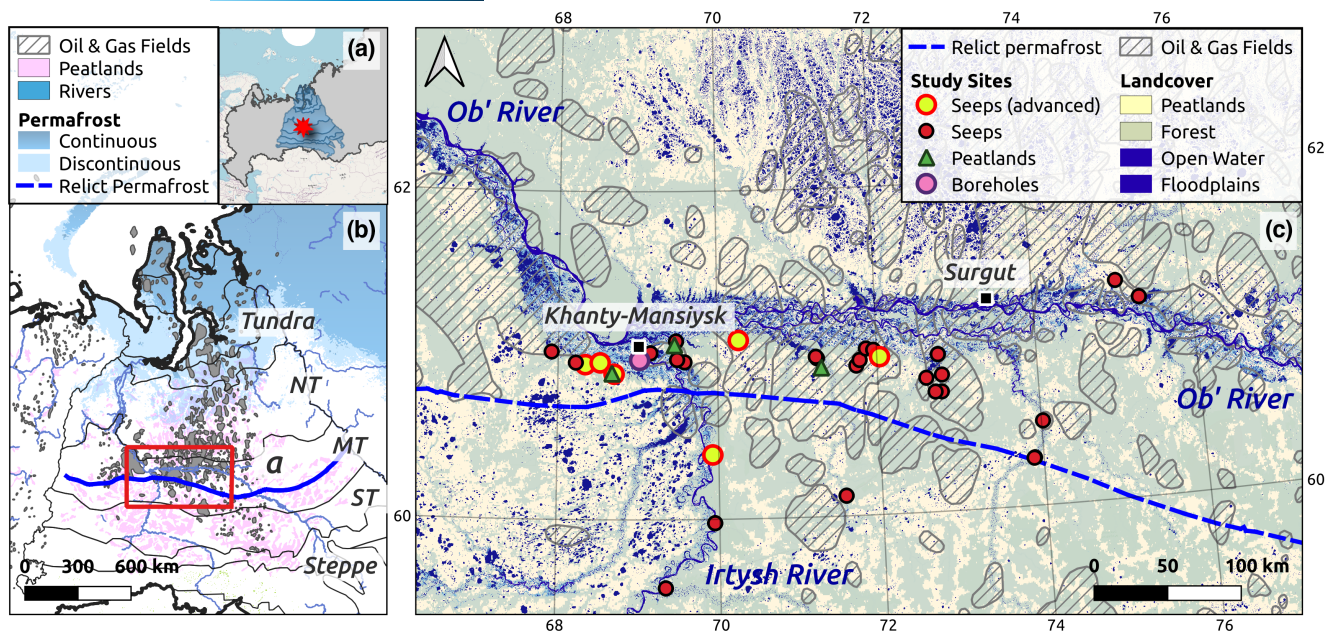
FIGURE 3 (a) Location of the study region in central Russia. (b) Map of the West Siberian Lowlands with red rectangle denoting the present study region. (c) Sampling site location. Permafrost zonation in this map was taken from Obu et al. (2018), version 5.0. Oil and gas fields' locations are indicated after Khafizov et al. (2022). Peatland cover is based on Lehner and Döll (2004). The southern border of relict permafrost was redrawn from Brown et al. (1997). Biome zonation is based on Terentieva et al. (2016). Notations "NT", "MT," and "ST" mean northern, middle, and southern subzones of taiga (boreal forests) biome. Open water and floodplain zones are based on Pekel et al. (2016). Forest cover is indicated after Shimada et al. (2014). Red dots indicate points where seep gas composition, dissolved gas concentration, pH, $\delta^{13}C(CH_4)$, $\delta D(CH_4)$, and $\delta D(H_2O)$ were investigated, red-yellow dots—where seep gas and water were also sampled to measure additional biogeochemical proxies including $T^{14}C$, dissolved organic carbon concentration, ^3H content and $\delta^{13}C(CO_2)$. Groundwater was sampled from Khanty-Mansiysk water supply wells. Map lines delineate study areas and do not depict accepted national boundaries.

Sphagnum-dominated raised bogs are widespread within the study region, and are characterized by ombrotrophic, acidic conditions with a pH less than 4.4. These nutrient-poor ecosystems are the result of the final stage of the paludification process. The region is abundant in forested bogs, with sparse stands of *Pinus sylvestris* reaching up to 10 m in height, and patterned bogs consisting of a mix of forested ridges and non-forested hollows and lawns (Kremenetski et al., 2003; Terentieva et al., 2016). The peat layer in these bogs typically ranges from 3 to 5 m in thickness, except for the youngest bogs, which can have a thickness as low as 1.5 m (Blanchet et al., 2017; Kremenetski et al., 2003; Masing et al., 2010; Turunen et al., 2001). Water-table levels (WTL), measured in centimeters from the moss surface, range from –15 cm in hollows and lawns to 70 cm in forested sites (WTL less than 0 indicates water levels above the moss).

The study region is also characterized by coniferous (*Pinus sibirica*, *Abies sibirica*, *Picea obovata*) and mixed conifer-deciduous forests that grow on terraces and well-drained areas along river valleys. These forests occur on acidic (pH <5.5) sandy-loam Podzols (as classified by the World Reference Base for Soil Resources) with low organic content (less than 2%) (Sabrekov et al., 2021). The groundwater level in these ecosystems is 5–7 m deep. Slopes along river valleys are covered by mixed and small-leaved aspen and birch (*Populus tremula*, *Betula pubescens*) stands that range from 10 to 20 m in height, with groundwater depths varying from 2 to 8 m.

2.2 | Study sites

We sampled 50 sites (Figure 3), mostly located on the floodplains of the Ob River and its tributaries. The locations of the sampled seeps were initially predicted using satellite imagery (Terentieva et al., 2022) and later confirmed through direct field surveys. We limited our study to sites that were accessible through the existing road network. Extensive sampling was carried out in August and September of 2020 to determine the origin of methane. Within each seep area, which is a water-logged bare depression in the floodplain, several individual seeps (small holes and craters releasing gas bubbles) were sampled. A total of six seep areas, which are briefly described in Table S1, were sampled in September of 2021 to measure the radiocarbon age of methane and other relevant biogeochemical parameters of the seeps. In addition, three typical peatlands located across the region were sampled in August and September of 2021 to serve as a representation of the gas source: Mukhrino (referenced in Alekseychik et al., 2017; Blanchet et al., 2017; Dyukarev et al., 2021), Chistoe (Kosykh et al., 2008), and Lempino (Kosykh et al., 2008). A brief description of the bog sampling sites is provided in Table S1. Finally, groundwater was taken from three active water supply wells (at depths of 25, 70, and 210 m) in Khanty-Mansiysk (latitude 61.091° N, longitude 69.465° E, elevation 37 m above sea level) in September of 2020.

The field sampling is described in Appendix S1. Briefly, bubbling gas from seeps was sampled using inverted funnels filled with seep water and held manually above the seep (Figure S1). Gas was sucked into the syringe and then transferred into 20 mL Hungate borosilicate glass vials (Bellco Glass, USA). Water discharging from the seep was sampled from exactly the same spot using 50 mL polypropylene syringe (KDM, Germany), triple-rinsed with seep water before sampling. Water was filtered in a few hours after sampling into 20 mL Hungate borosilicate glass vials (Bellco Glass, USA) through single-use 0.2 μm acetate cellulose filter units (Corning, USA).

2.3 | Selection of biogeochemical tools

We chose a set of biogeochemical indicators to determine which gas-origin hypotheses is correct (Table 1). This set included light hydrocarbons (C_1–C_5), CO_2 gas contents, and stable-isotope compositions of methane carbon $\delta^{13}C(CH_4)$, hydrogen $\delta D(CH_4)$, and water hydrogen $\delta D(H_2O)$ as a source of hydrogen for methane. We measured these indicators at the 50 sites we visited (Figure 3, red dots). For the six sites with the most active bubbling (Figure 3, yellow dots), we also determined stable-isotope composition of carbon in carbon dioxide $\delta^{13}C(CO_2)$, DOC concentration as well as radiocarbon age of methane $T^{14}C$.

Briefly, radiocarbon-free thermogenic or secondary microbial methane would support the H1 hypothesis, where seep methane is uplifted from underlying oil and gas reservoirs. Radiocarbon-free primary microbial methane would support the H2 hypothesis, where methane is sourced from degrading permafrost. Here, H1 and H2 could be differentiated by the stable isotope compositions of methane and associated CO_2: $\delta^{13}C(CH_4) > -50‰$ and $\delta^{13}C(CO_2) > +15‰$ would argue in favor of the secondary microbial origin (H1), while $\delta^{13}C(CH_4) < -60‰$ and $\delta^{13}C(CO_2) < +2‰$ would support primary microbial origin (Milkov & Etiope, 2018). Values in between would indicate mixed origin. Finally, radiocarbon-rich primary microbial methane co-occurring with $\delta^{13}C$-depleted CO_2 and negligible amounts of ethane and propane would support the H3 hypothesis, where methane comes from adjacent raised bogs. However, it should be noted that these tools could not determine whether the relict permafrost degradation contributed to a migration of the thermogenic methane from petroleum-bearing sediments. If such migration took place, the applied geochemical tools would not be able to determine whether the permafrost acted as a cap or not.

To minimize the uncertainty in determining the origin of methane, we utilized reference values for hypothesized sources in the study region as described in Table 1. Data for thermogenic gas in the study region's reservoirs were obtained from Goncharov et al. (2005) and Milkov (2010). Since there were no data available on methane that may be trapped in the relict permafrost in the West Siberian Lowlands, we used data from Kraev et al. (2019) and Rivkina et al. (2007) as the best-available proxy. These studies indicate that $\delta^{13}C(CH_4)$ in different permafrost layers ranges from −64‰ to −99‰. The characteristics of peatland gas, including methane

TABLE 1 Geochemical tools for determination of gas origin in Western Siberia boreal zone seeps.

Parameter	Seep CH_4 sourced from			Sources
	Hydrocarbon reservoirs	Degrading relict permafrost	Raised bogs	
Origin based on $\delta^{13}C(CH_4)$ and $\delta D(CH_4)$ as depicted in Figure 4a	Thermogenic or secondary microbial	Primary microbial; $\delta^{13}C(CH_4)$ from −64‰ to −99‰	Primary microbial	Range for $\delta^{13}C(CH_4)$ in the relict permafrost from Kraev et al. (2017, 2019) and Rivkina et al. (2007); genetic fields from Milkov and Etiope (2018)
Radiocarbon age, $T^{14}C$	No radiocarbon	No radiocarbon	<12,000 years (age of basal peat in raised bogs of the region)	Peat age data from Kremenetski et al. (2003), Turunen et al. (2001) and Zarov et al. (2021)
$\delta^{13}C(CO_2)$ as indicator of biodegradation	> +2‰ for secondary microbial; < +10‰ for thermogenic	< +15‰	−10 to −25‰ (as in raised bogs of the region, sampled in this study)	Limit for primary microbial CH_4 from Aravena et al. (1993), Clymo and Bryant (2008) and Shoemaker and Schrag (2010), limits for secondary microbial and thermogenic CH_4 from Milkov (2018) and Milkov and Etiope (2018)
$CH_4/(C_2H_6+C_3H_8)$ ratio	>2 for secondary microbial; >0.1 for thermogenic	>200	>200	Milkov and Etiope (2018)

Note: Values confirming certain hypothesis can overlap for almost all indicators; any of the hypothesis could be confirmed only when all indicators have values specified for this hypothesis.

concentration, $\delta^{13}C(CH_4)$, $\delta D(CH_4)$, $\delta^{13}C(CO_2)$, and $\delta D(H_2O)$ were measured and presented in this study. Finally, groundwater from three active water supply wells was sampled to investigate its role in methane migration to seeps.

2.4 | Chemical and isotopic analyses

The gas samples were analyzed for light hydrocarbons (C_1–C_5) and CO_2 simultaneously using a gas chromatograph Crystall-5000 (Chromatec, Russia). The gas chromatograph was equipped with flame ionization and thermal conductivity detectors, operated at methane concentration below and above 5000 ppm (0.5%), respectively. To determine the concentrations of dissolved gases in peat porewater and groundwater, the headspace method was utilized (Hope et al., 1995). For a better comparison with CH_4 and CO_2 contents in gas from seeps, we presented dissolved gas concentrations in % of total water saturation at in situ temperature and pressure, calculated using (Clymo & Bryant, 2008; Sander, 2015). Further details about the laboratory methods are described in Appendix S1.

Stable isotope compositions of carbon and hydrogen in methane, carbon in carbon dioxide, and hydrogen in water were measured using gas chromatography isotope ratio mass spectrometry. The results reported are an average of three replicates. All stable isotope ratios are reported at a permil scale in the δ-notation relative to Vienna Standard Mean Ocean Water (VSMOW) for $\delta D(CH_4)$ and $\delta D(H_2O)$ and Vienna Pee Dee Belemnite (VPDB) for $\delta^{13}C(CO_2)$ and $\delta^{13}C(CH_4)$. IAEA-CH-7 polyethylene foil (International Atomic Energy Agency, 2022, Austria) was used as a calibration standard. The repeatability was less than ±0.1‰ for $\delta^{13}C$ and ±1.0‰ for δD in gases and less than ±0.3‰ for δD in water (Dubinina et al., 2019). Given values are an average of three replicates. The apparent stable isotope fractionation factor for a reaction A→B is reported as α (A−B):

$$\alpha(A-B) = \frac{\delta A + 1000}{\delta B + 1000}$$

and also as isotopic enrichment factor $\varepsilon \equiv 1 - \alpha$ (in permil).

Methane radiocarbon dating was performed by accelerator mass spectrometry (AMS) in the AMS Golden Valley laboratory (Novosibirsk, Russia; laboratory code GV). Seep gas was graphitized using the absorption-catalytic unit as described in Lysikov et al. (2018). Obtained powder containing 2–3 mg of carbon was compressed into tablets and analyzed by AMS (Parkhomchuk & Rastigeev, 2011). In addition to seep gas samples, the graphitization was also conducted for standard samples: US National Bureau of Standards Oxalic Acid I (OX-I) and Australian National University Sucrose (ANU). The relative content of radiocarbon $^{14}C/^{13}C$ in samples was normalized to the content of $^{14}C/^{13}C$ in the standards taking into account their stable isotope compositions ($\delta^{13}C = -19.0$ and -10.8‰ for OX-I and ANU, respectively). Fine-grained porous graphite of coke-pitch composition, processed through the same graphitization procedure as the samples, was used as a blank. All ^{14}C ages were calibrated using OxCal v. 4.4.2 (Bronk Ramsey, 2009) and the IntCal20 atmospheric curve (Reimer

et al., 2020). Sample AMS numbers are given in Table S1. The fraction modern ($F^{14}C$, dimensionless) corrected for the stable isotope compositions of seep gas ($\delta^{13}C_{seep} \equiv \delta^{13}C(CH_4)$, ‰) and blank ($\delta^{13}C_{blank}$, ‰) samples was calculated by:

$$F^{14}C = \frac{pMC_{seep}}{100 \cdot \left(1 + 2 \cdot \frac{\delta^{13}C_{seep}}{1000}\right)} - \frac{pMC_{blank}}{100 \cdot \left(1 + 2 \cdot \frac{\delta^{13}C_{blank}}{1000}\right)}$$

where pMC_{seep} and pMC_{blank} are measured fractions of modern carbon in seep gas and blank sample, respectively (%). Radiocarbon age ($T(^{14}C)$, years before present (BP)) was determined from the fraction modern using:

$$T(^{14}C) = -8033 \cdot \ln\left(F^{14}C\right)$$

Tritium measurements were performed in the laboratory of nuclear oceanology of V.I.Il'ichev Pacific Oceanological Institute, Far Eastern Branch, Russian Academy of Sciences (Vladivostok, Russia) on the QUANTULUS 1220 ultralow level liquid scintillation counter (Perkin Elmer, USA) as described in Gröning and Rozanski (2003) and Morgenstern and Taylor (2009). The water samples were distilled with $KMnO_4$, then alkalized with Na_2O_2 and enriched electrolytically prior to analysis. We estimated the seep groundwater residence time using measured tritium content by a simple numerical model of steady-state well-mixed homogeneous aquifer (Cook, 2020; Jean-Baptiste et al., 2017), described in detail in Appendix S2.

DOC concentrations were measured as non-purgeable organic carbon (NPOC) via high temperature catalytic combustion (vario TOC cube, Elementar Analysensysteme GmbH, Germany) with an uncertainty of 2% and a detection limit of 0.03 mgC l^{-1}. Values are given as a mean of three replicates. Acidity (pH) as well as dissolved oxygen concentration in seep water were measured in situ using HI 98129 and HI 9147-04, respectively (both Hanna Instruments, USA).

2.5 | Methanogenic pathway identification

The study employed three models to predict the apparent enrichment factor of hydrogen in methane in relation to the accompanying water. The first model, proposed by Whiticar (1999), is based on the metabolic pathway as the primary control for $\delta D(CH_4)$. The other two models (Douglas et al., 2021; Waldron et al., 1999) consider $\delta D(H_2O)$ to be the primary determinant of $\delta D(CH_4)$ in global wetlands. In sulfate-poor boreal wetlands, including those in the West Siberia, acetate fermentation is the dominant process (Conrad, 2020; Kotsyurbenko et al., 2004; Lokshina et al., 2019), making the latter models a suitable representation of this pathway. The former model, on the other hand, directly predicts δD of methane generated through the CO_2 reduction pathway (Golding et al., 2013). Since methylotrophic methanogenesis is not considered to play a significant role in CH_4 production in non-saline environments (Conrad, 2020), the relative contributions of these two major methanogenic pathways can be estimated through mass balance:

$$\delta D(CH_4)_{meas} = f_{CR} \cdot \delta D(CH_4)_{mod,CR} + (1 - f_{CR}) \cdot \delta D(CH_4)_{mod,AF}$$

where $\delta D(CH_4)_{meas}$, $\delta D(CH_4)_{mod,CR}$, $\delta D(CH_4)_{mod,AF}$ are stable isotope compositions of hydrogen in methane measured in the field, modeled for CO_2 reduction and modeled for acetate fermentation, respectively (‰), and f_{CR} is a relative contribution of CO_2 reduction pathway (dimensionless). From this equation, f_{CR} can be written as:

$$f_{CR} = \frac{\delta D(CH_4)_{meas} - \delta D(CH_4)_{mod,AF}}{\delta D(CH_4)_{mod,CR} - \delta D(CH_4)_{mod,AF}}$$

$\delta D(CH_4)_{mod,CR}$ is calculated according to Whiticar (1999) using measured value of $\delta D(H_2O)$ for seep water, $\delta D(H_2O)_{meas}$:

$$\delta D(CH_4)_{mod,CR} = \delta D(H_2O)_{meas} - 160$$

$\delta D(CH_4)_{mod,AF}$ is calculated by regression models from Douglas et al. (2021) and Waldron et al. (1999) trained on data measured in wetlands. Since these models are based on similar datasets, we use average among them:

$$\delta D(CH_4)_{mod,AF} = 0.5 \cdot (0.675 \cdot \delta D(H_2O)_{meas} - 284) + 0.5 \cdot (0.53 \cdot \delta D(H_2O)_{meas} - 297.7)$$

The contribution of the CO_2 reduction pathway could be underestimated in our analysis since the models from Douglas et al. (2021) and Waldron et al. (1999) may not exclusively represent the acetate fermentation pathway. These models are based on in situ data from freshwater wetlands where methane production via the CO_2 reduction pathway can also play a significant role (Conrad, 2020; Kotsyurbenko et al., 2004; Lokshina et al., 2019). However, since we do not have samples with $\delta D(CH_4)$ values outside the range predicted by these models (as seen in Figure S2), their accuracy for our data is considered acceptable. We exclude from analysis those gas samples, which were taken from seeps submerged by river water, to ensure that there is no admixtures of allochthonous water or CH_4.

2.6 | Statistical analyses

All calculations were performed using MATLAB 2022a (The MathWorks, USA). Significant differences ($p < .05$) between two groups were evaluated using the two-tailed Wilcoxon rank sum test (*ranksum*). Linear regression models were evaluated using *fitlm*.

3 | RESULTS

3.1 | Seep gas composition

The characteristics of the gas and water discharging from seeps are detailed in Table 2. Additional biogeochemical information for six sites is found in Table 3. The gas composition was dominated by methane and nitrogen, with carbon dioxide, ethane, and propane being minor components. Dissolved oxygen was not detected in any of the samples, with concentrations below the threshold sensitivity of $0.1\,mg\,L^{-1}$. The CH_4 concentration in the seep gas varied from 0.04% to 67.2%, while the concentration of ethane and propane never exceeded 0.02%. As a result, methane made up more than 99.9% of the hydrocarbons in the gas from all seeps. CO_2 concentrations in seep water were significantly lower ($p = .0071$, $N = 37$) when dissolved CH_4 concentrations were less than 0.3 mM: median dissolved CO_2 concentrations were 0.41 mM and 1.06 mM in samples with methane concentrations less and more than 0.3 mM, respectively (Figure S3). The medians of pH for seeps methane concentrations less and more than 0.3 mM were almost identical ($p = .86$).

The highest dissolved methane concentration in the peat porewater was observed at a depth of 2 m in Mukhrino and Lempino bogs, with a concentration of up to 68.4% of total saturation at in situ temperature. In the overlying peat layers, the concentration of dissolved methane ranged from 15.3% to 36.7% (Figure S4). Dissolved CO_2 concentration varied in the peat porewater from 2.3% to 9.2% without pronounced depth trend (Figure S5). The median concentration

TABLE 2 Overview of geochemical parameters for gas and water in seeps and peatlands.

Parameter	Median ± IQR		Minimum		Maximum	
	Seeps	Peatlands	Seeps	Peatlands	Seeps	Peatlands
CH_4 concentration, %	30.3 ± 43.2	30.9 ± 13.0	0.039	15.3	67.2	68.4
CO_2 concentration**, %	0.86 ± 0.79	2.5 ± 0.8	0.17	0.60	3.0	2.8
$CH_4/(C_2H_6 + C_3H_8)$	47,812 ± 98,991	n.d.	4487	n.d.	437,200	n.d.
$\delta^{13}C(CH_4)$***, VPDB ‰	−79.3 ± 14.2	−68.1 ± 6.5	−98.3	−76.3	−64.6	−57.9
$\delta^{13}C(CO_2)$**, VPDB ‰	−23.3 ± 4.3	−15.3 ± 4.0	−29.6	−20.8	−20.3	−7.7
$\delta D(CH_4)$*, VSMOW ‰	−304.8 ± 47.0	−286.2 ± 13.8	−354.2	−329.4	−270.6	−275.5
$\delta D(H_2O)$**, VSMOW ‰	−119.2 ± 10.1	−106.2 ± 7.5	−130.7	−115.0	−103.4	−98.0
pH***	6.8 ± 0.5	4.2 ± 0.6	6.2	3.3	8.6	4.7

Note: Asterisks denote significant (*$p < .01$, **$p < .001$, ***$p < .0001$) differences between seep and peatland median values of respective parameters; peatland gas concentrations are recalculated from dissolved concentrations using Henry's law; n.d. means no data.

TABLE 3 Additional biogeochemical parameters of water and gas at selected seep sites.

Site	$\delta^{13}C(CO_2)$, VPDB ‰	$\alpha^{13}C$ (CO_2-CH_4)	$T(^{14}CH_4)$, years BP	DOC, mgC l^{-1}	$^3H \pm 2\sigma$, T.U.	Renewal time[a] $\pm 2\sigma$, years
Bolshaya Rechka river	−23.39	1.0670	6926 ± 132	8.3	1.61 ± 0.26	569 ± 90
Baibalak channel of Ob	−28.71	1.0572	7340 ± 140	11.0	0.28 ± 0.13	3400 ± 2000
Bolshoy Variegan river	−22.68	1.0626	7975 ± 186	7.7	10.01 ± 0.76	44 ± 10
Elykovskaya river	−23.26	1.0573	6436 ± 120	n.d.	4.54 ± 0.38	172 ± 18
Mukhrino creek	−20.30	1.0588	4204 ± 111	n.a.	n.a.	n.a.
Grishkina channel of Irtysh	−29.60	1.0727	4586 ± 112	10.5	0.62 ± 0.22	1530 ± 400
Yarki stream	−20.66	1.0763	n.d.	5.0	7.33 ± 0.49	86 ± 9
Shaitanka river	−25.71	1.0641	n.d.	3.9	18.65 ± 0.86	1 ± 1

Note: n.d.—no data (lost samples), n.a.—not applicable (seep was inundated by allochthonous river water).

[a]Calculated based on seep water tritium content, see Appendix S2 for details.

of carbon dioxide in the gas phase was significantly lower in seeps compared to peatlands ($p < .0001$, $N = 52$).

The groundwater in the studied region was also highly saturated with methane, with the concentration increasing from $4.3 \pm 0.4\%$ (average ± SD) at 25 m depth to $35.2 \pm 2.4\%$ at 70 m and $27.7 \pm 5.9\%$ at 215 m depth, respectively. Ethane was not detected in the groundwater in concentrations exceeding 0.01%, and propane was not detected at all.

3.2 | Gas stable isotope composition

The stable isotope composition of methane from both seeps and groundwater in the studied area was primary microbial with a few samples showing isotopic signatures characteristic of thermogenic gas, but still within the biogenic field (Figure 4a). We found a clear linear trend ($p < 0.0001$, $R^2 = .63$, $N = 50$) between seep $\delta^{13}C(CH_4)$ and $\delta D(CH_4)$, where depletion in carbon heavy isotope corresponded to depletion in deuterium (Figure 4a). The concentration of methane in seep gas decreased along with a depletion of heavy carbon (Figure 4b) and hydrogen (data not shown) stable isotopes. The dominating methanogenic pathway is unclear from the genetic diagram, as the fields for acetate fermentation and CO_2 reduction overlap for the values observed in seeps and groundwater.

$\delta^{13}C(CH_4)$, $\delta D(CH_4)$, and $\delta D(H_2O)$ were significantly more enriched in peatland gas compared to seep gas ($p < .0001$, $N = 74$, $p = .0027$, $N = 72$, and $p = .0001$, $N = 39$, respectively). However, their values overlapped and maximal values are closer than minimal (Table 2). In some samples, peatland methane reached the range of thermogenic gas on genetic diagram. The correlation between $\delta^{13}C(CH_4)$ and methane concentration in peatlands was significant, but less pronounced compared to the correlation observed in seeps (Figure 4b). Groundwater methane showed stable isotope fingerprints similar to those of seep methane, but more depleted in ^{13}C and/or enriched in D.

The $\delta^{13}C(CO_2)$ values were different between peatland and seep gas samples ($p = .0002$, $N = 23$). In seep gas, $\delta^{13}C(CO_2)$ ranged

from −20.3‰ to −29.6‰ (as reported in Table 3). The $\delta^{13}C(CO_2)$ in peatlands varied from −20.8‰ to −7.7‰, decreasing with depth (Figure S6). As $\delta^{13}C(CH_4)$ also tended to decrease with depth (as seen in Figure S7), $\delta^{13}C(CO_2)$ had a positive correlation ($p = .0009$, $N = 13$, $R^2 = .64$) with $\delta^{13}C(CH_4)$ in co-occurring peatland gases (Figure S8).

3.3 | Methanogenic pathway identification

The observed δD in peat porewater ranged from −98.0 to −115.0‰ (Table 2), and tended to decrease with depth (Figure S9). The difference in δD between seep water and co-occurring methane was approximately 167‰, 186‰, and 224‰ for the maximal, median, and minimal values, respectively. These values aligned with those found in peat porewater, which were 178‰, 193‰, and 224‰, respectively. Isotopic composition of hydrogen in seep methane significantly correlated with isotopic composition of hydrogen in co-occurring water (Figure S2). However, slope was steeper than predicted by either metabolic pathway fractionation model. The estimated relative contribution of the CO_2 reduction pathway (f_{CR}) ranged from 0.15 to 0.98, with a median of 0.71. The f_{CR} significantly correlated with methane concentration in seep gas and $\delta^{13}C(CH_4)$ (Figure 5a,b). Relative contribution of the CO_2 reduction pathway in peatlands significantly increased with depth ($p = .025$, $N = 10$).

3.4 | $^{14}CH_4$ age and additional geochemical tools

The observed values of methane's radiocarbon age, as listed in Table 3, showed a wide range from 4.2 to 8.0 thousand years BP with a median of 6.7 thousand years BP. Thus, organic carbon used for methane production by *Archaea* was of early to mid-Holocene age. The apparent stable isotope fractionation factor $\alpha^{13}C(CO_2-CH_4)$ in seep gases ranged from 1.0572 to 1.0727 (Table 3), with a median of 1.0607. The $\alpha^{13}C(CO_2-CH_4)$ in peatland gas was statistically similar ($p = .1078$, $N = 20$ for median comparison) with a range of 1.0475–1.0703 and a median of 1.0570.
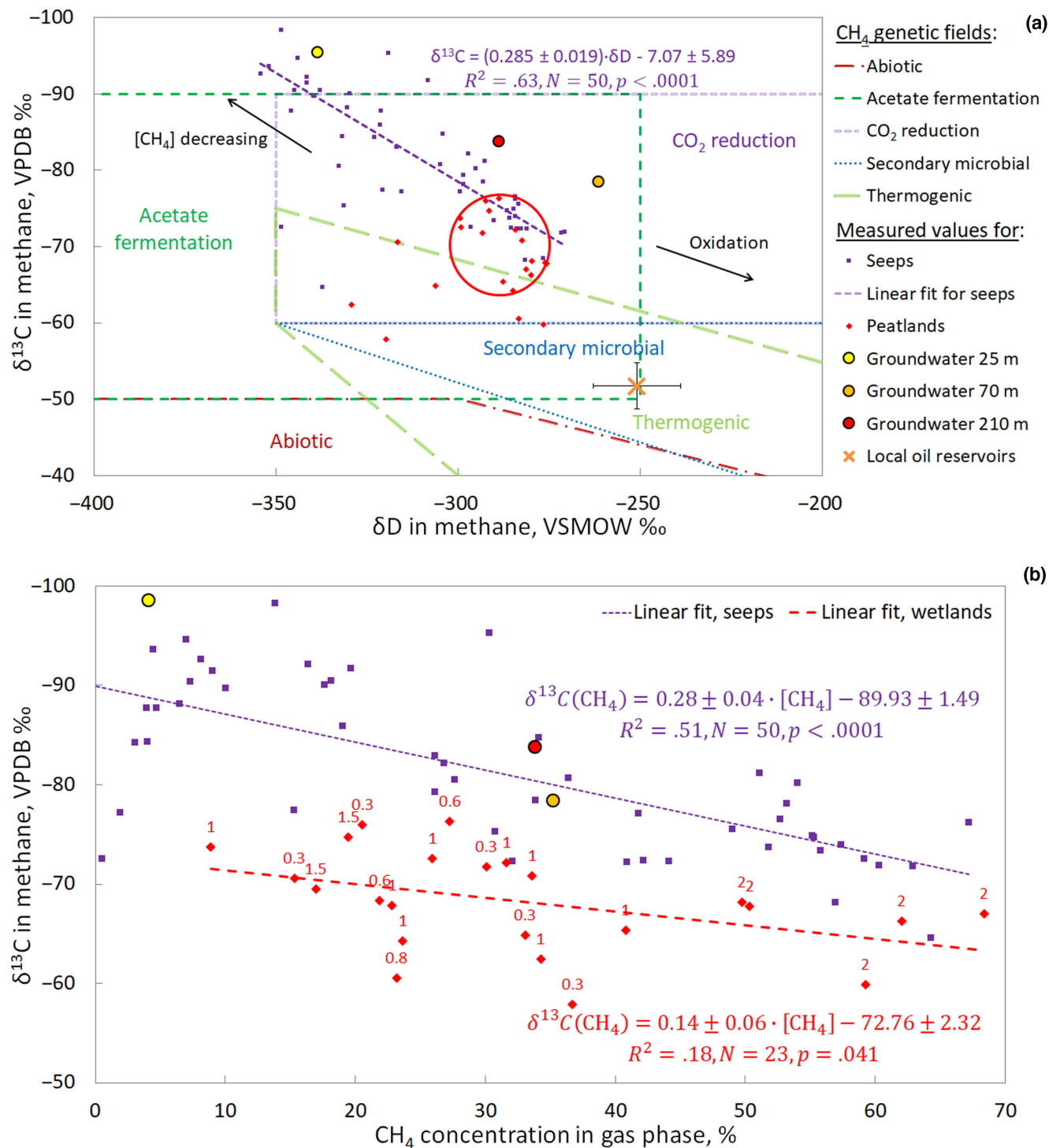
FIGURE 4 (a) A genetic diagram of the stable isotope composition of methane from various sources in Western Siberia's boreal zone. Fields are redrawn from Milkov and Etiope (2018). The majority of the seep and groundwater samples showed isotopic signatures consistent with primary microbial methane. The red circle highlights the region of overlapping methane stable isotope compositions of seeps and peatlands. Seep methane with isotope fingerprints inside of this circle is likely produced in situ in peatlands. Seep methane, which is depleted relative to red circle region, could be at least partly produced in groundwater. (b) The isotopic depletion of seep methane with decreasing methane concentration. Numbers indicate peat depth (in m) where sample was taken. This, along with the observed linear trend between $\delta^{13}C(CH_4)$ and $\delta D(CH_4)$, indicates minimal oxidation of methane occurred during migration from bogs to seeps.

The tritium content in seep water ranged from 0.26 to 18.65 T.U., with a median value of 4.54 T.U. Using a simple steady-state model to assess tritium dynamics in a well-mixed aquifer, we predicted that the groundwater renewal time for methane-bearing aquifers in the Western Siberia boreal zone region can vary widely, ranging from 1 to 3400 years (Table 3) with a median of 172 years.
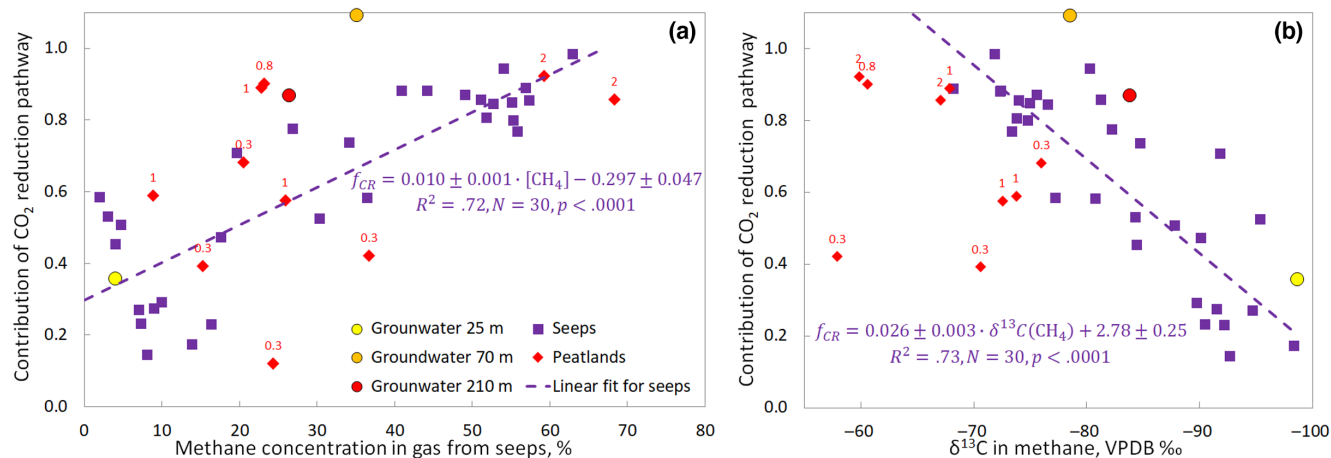
FIGURE 5 The relative contribution of the CO_2 reduction methanogenic pathway in seeps, peatlands, and groundwater with varying (a) methane concentrations and (b) $\delta^{13}C(CH_4)$. The dashed lines indicate linear fits for seeps. Numbers indicate peat depth where sample (in m) was taken. The linear correlation between pathway contribution and methane concentration and $\delta^{13}C(CH_4)$ in seep-gas samples indicates a mixing of two methane sources dominated by different pathways. CO_2 reduction accounted for 75%–100% of ^{13}C-enriched seep methane in high-concentration samples, while acetate fermentation contributed substantially to ^{13}C-depleted methane in low-concentration samples.

4 | DISCUSSION

4.1 | Methane origin

Peatlands (H3) are the key source of methane released from terrestrial seeps in the West Siberian Lowlands. Several lines of evidence support this conclusion. The maximal and median methane concentrations were similar in seep and peatland gas samples. Methane comprised over 99.9% of hydrocarbons in the seep gas (Table 2) as typical for its microbial origin (Etiope, 2015). Trace amounts of ethane and propane are also consistent with Hypothesis 3 as these hydrocarbons can be produced by microbes (Milkov & Etiope, 2018; Oremland et al., 1988; Xie et al., 2013). The absence of alkanes with more than three carbon atoms suggests that the seep gas is not of thermogenic origin (Etiope, 2015). The stable isotope compositions of both carbon and hydrogen in the methane indicate that it is of the primary microbial origin (Figure 4a). Radiocarbon age of the seep methane reflects its origin from early to mid-Holocene organic matter and is lower than the basal peat organic carbon ages in peatlands of the region (Kremenetski et al., 2003; Turunen et al., 2001; Zarov et al., 2021). Stable isotope composition of CO_2 in seep gas provides further evidence for the peatland origin of seep methane, as the CO_2 is believed to come from the same source. The $\delta^{13}C$-depleted CO_2 in the seep gas contradicts the possibility of secondary microbial methane percolation from petroleum-bearing sediments into surface aquifers: CO_2 produced during petroleum biodegradation is strongly $\delta^{13}C$ enriched, with values up to +40‰ (Milkov & Etiope, 2018).

The significant differences in pH, carbon dioxide concentration, and $\delta^{13}C(CO_2)$ between seeps and peatlands of the studied region (Table 2) suggest the interaction between acidic peat porewater and calcite in the mineral layers underlying peat deposits. Ca^{2+} and HCO_3^- are the dominant ions in the groundwater of the region, reflecting the dissolution of carbonate minerals from the underlying

rocks and sandstone cements (Frey et al., 2007). We hypothesize that acidic bog porewater is buffered by calcite dissolution after mixing with groundwater, according to the following reaction (Clark & Fritz, 2013):

$$CO_2 + H_2O + CaCO_3 \rightarrow Ca^{2+} + 2HCO_3^-$$
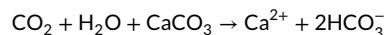
This mechanism can explain decrease in the carbon dioxide concentrations compared to bog porewater and simultaneous increase in pH. Furthermore, this mechanism successfully predicts observed $\delta^{13}C$-depletion of CO_2 in seep gas compared to peatland gas accompanying this buffering. The isotope composition of the remaining substrate $\delta_s^{13}C(CO_2)$ (i.e., of seep gas) should follow the Rayleigh model of fractionation (Clark & Fritz, 2013):

$$\delta_s^{13}C(CO_2) = \delta_0^{13}C(CO_2) + \varepsilon^{13}C(HCO_3^- - CO_2) \bullet \ln(f)$$

where $\delta_0^{13}C(CO_2)$ is the isotope composition of CO_2 carbon at the start of the process (i.e., in peatland gas), $\varepsilon^{13}C(HCO_3^- - CO_2)$ is the enrichment factor between hydrocarbonate as a product and carbon dioxide in gas phase as a substrate (‰) and f is the fraction of unreacted CO_2 (dimensionless). Under equilibrium conditions $\varepsilon^{13}C(HCO_3^- - CO_2)$ is 10.2‰ at 5°C (Clark & Fritz, 2013). Assuming f is a ratio of seep to peatland median gas phase CO_2 concentrations (0.86/2.50=0.34) and $\delta_0^{13}C(CO_2)$ is a median $\delta^{13}C(CO_2)$ in the catotelm (>1 m deep) gas (−14.0‰), $\delta_s^{13}C(CO_2)$ would be −24.9‰. The minor differences between this and observed median value (−23.3±4.3‰) may have arisen because the gas samples were collected only from the upper peat layers. In deeper peat layers (>2 m), the substrate $\delta_0^{13}C(CO_2)$ could be more enriched in heavy isotopes, as has been observed in other peatlands (Aravena et al., 1993; Clymo & Bryant, 2008; Shoemaker & Schrag, 2010). In addition, ^{13}C-depleted carbon dioxide in the seep gas indicates minor role of methane production in groundwater through

CO_2 reduction. If this process was significant, then CO_2 would be enriched relative to the calculated equilibrium value.

In an earlier study of West Siberian floodplain seeps, Oshkin et al. (2014) reported higher methane concentrations (70%–99%), but similar $\delta^{13}C(CH_4)$ (−71.1 to −71.3‰) compared to this study. We do not have a natural explanation of these differences in methane concentration. Oshkin et al. (2014) used flame ionization detector to measure methane concentrations in the seep gas, but did not report in what range it was calibrated. Linear response of the flame ionization detector could be limited under concentrations of more than 5% (McNair et al., 2019). The narrow range of $\delta^{13}C(CH_4)$ values can be explained by the much smaller spatial extent of the Oshkin et al. (2014) study (a single 3-km long stretch of river floodplain). Methane in all individual seeps of this area likely migrated from the same peatland and thus had almost identical isotope fingerprints.

4.2 | Methane transport from raised bogs to seeps

Seep methane radiocarbon age comprises the age of organic matter used for CH_4 production and migration time of CH_4 from peatlands to the seeps. The early to mid-Holocene radiocarbon age of seep methane could be solely explained by the age of organic matter at depths of 1.5–4 m in West Siberian peatlands (Kremenetski et al., 2003; Turunen et al., 2001; Zarov et al., 2021). If seep methane is indeed produced in these deep peat layers, then methane migration time should be negligible relative to its age. The time of methane migration from source to seep is the sum of individual methane residence times in the peat layers, underlying aquitard(s), and aquifer(s). It is largely dependent on the transport mechanism, which can be either predominantly advective (Glaser et al., 2016; Reeve et al., 2009) or diffusive (Beer & Blodau, 2007; Clymo & Bryant, 2008; Shoemaker & Schrag, 2010). When the underlying aquitard has very low hydraulic conductivity, solute transport is restricted to molecular diffusion both in the deeper peat (Beer & Blodau, 2007; Fraser et al., 2001; Reeve et al., 2000) and the aquitard (Jacobs et al., 2013). In contrast, solutes can move downward from the surface to the deeper peat by advection, when underlying deposits are relatively permeable (Reeve et al., 2009). It is noteworthy that in advection-dominated raised bogs, deeper-peat methane production is at least partly fueled by recently photosynthesized organic matter; this methane is typically half the age of the peat at any given depth (Aravena et al., 1993; Chanton et al., 1995; Glaser et al., 2016). Hence, fast migration via advective transport, which is suggested to occur on a decadal timescale (Glaser et al., 2016), would likely result in seep methane age of less than 2–4 thousand years BP, half the average age of the peat at depths of 1.5–4 m in West Siberian boreal zone (Kremenetski et al., 2003; Turunen et al., 2001; Zarov et al., 2021).

After migration through peat layers and aquitard(s), methane is transported by groundwater, which partly discharges in seeps. Seep water ^3H data clearly indicate that the contribution of groundwater transport to the age of the seep methane is minor. Residence time of groundwater discharging in seeps (median is 172 years) is more than one order of magnitude lower than seep $^{14}CH_4$ age (Table 3). The presence of tritium with activities above approximately 1 T.U. in water from seeps suggests that post-1953 precipitations is reaching the aquifer(s) discharging in seeps (Jasechko, 2019). Nevertheless, the variability in tritium content of seep water suggests that in some cases, groundwater transport may significantly (up to several thousand years) contribute to the age of seep methane.

One more line of evidence contradicting the fast-migration mechanism is based on the depth trend of stable isotopes in CH_4 and CO_2 in peatlands. Since methane in studied peatlands was produced dominantly via CO_2 reduction (Figure 5), CO_2 isotope composition directly affect $\delta^{13}C(CH_4)$. The $\delta^{13}C(CO_2)$ values in studied peatlands increase with depth and are positively correlated with the $\delta^{13}C(CH_4)$ values (Figure S8). Several studies have reported the simultaneous increase in $\delta^{13}C(CO_2)$ and $\delta^{13}C(CH_4)$ with depth in peatlands (Aravena et al., 1993; Clymo & Bryant, 2008; Corbett et al., 2015). Hence, if deeper (>1.5 m) peat layers would significantly contribute to the production of seep methane, $\delta^{13}C(CH_4)$ in seeps would be higher than observed, that is, higher than −63.6 ± 4.3‰ (average ± SD for the depth of 2 m). Notably, it was not the case for $\delta D(CH_4)$ because source water was not enriched but slightly depleted in heavier hydrogen isotopes with depth (Figure S7). This difference in depth trends of $\delta^{13}C(CO_2)$ and $\delta D(H_2O)$ in peatlands is a viable explanation why methane in seeps had a higher maximal $\delta^{13}C(CH_4)$ but a lower maximal $\delta D(CH_4)$ compared to peatlands (Table 2). As the change in $\delta^{13}C(CH_4)$ in peatlands with depth relative to the whole range of observed $\delta^{13}C(CH_4)$ values for seeps is more pronounced than change in $\delta D(H_2O)$ for $\delta D(CH_4)$, differences in $\delta^{13}C(CH_4)$ between peatland and seep methane provide more insights on seep methane transport and origin.

Therefore, both current knowledge on peatland hydrology and depth trends of $\delta^{13}C(CH_4)$ in studied peatlands contradict the fast-migration explanation of methane via advective transport. Otherwise, seep methane would be more $\delta^{13}C$ enriched and would be younger than observed. Transport of methane by groundwater is likely too fast to significantly contribute to the seep methane age. By elimination, it could be suggested that diffusion through deeper peat layers and underlying aquitard is the primary determinant of the seep methane age.

4.3 | Biogeochemical processes driving concentration of seep methane

The isotopic depletion of seep methane with decreasing methane concentration (Figure 4) indicates that no significant oxidation of methane occurred during migration from bogs to seeps. Oxidation drives isotope composition of methane toward more enriched values with a slope between $\delta^{13}C(CH_4)$ and $\delta D(CH_4)$ from 0.05 to 0.2 tending to be larger for aerobic than for anaerobic methane oxidation (Kinnaman et al., 2007; Rasigraf et al., 2012; Whiticar, 2020). Both the aerobic and anaerobic methane oxidation are likely impeded by the absence of dissolved oxygen and low concentrations

of alternative electron acceptors (Oshkin et al., 2014) observed in the groundwater of the study region, respectively. Diffusion of methane from gas bubbles to the groundwater also cannot explain the observed depletion. Otherwise, a fractionation slope between $\delta^{13}C(CH_4)$ and $\delta D(CH_4)$ would be about 1 (Bergamaschi, 1997).

The pronounced linear correlations between pathway contribution and methane concentration as well as $\delta^{13}C(CH_4)$ in seep gas samples (Figure 5) suggest a continual mixing of two methane sources dominated by different pathways. The first source produces $\delta^{13}C$-enriched (–70 to –75‰, Figure 5b) seep methane with higher concentrations (45%–60%, Figure 5a) predominantly via CO_2 reduction. This seep methane had CH_4 stable isotope fingerprints (red circle in Figure 4a) and concentration values (Figure 4b) similar to methane in upper 1–2 m of raised bogs. This similarity indicates that methanogenesis in bogs is an appropriate candidate for the first source. Consistent with this, CO_2 reduction is suggested to be a dominant methanogenic pathway in the catotelm of raised bogs (Conrad, 2020; Hornibrook et al., 1997; Kotsyurbenko et al., 2004) below the root zone, where transport of methane to the atmosphere is limited (Laanbroek, 2010). If this methane with higher concentrations was produced not in peatlands but in groundwater or floodplains, then CO_2 in a seep gas would be not depleted but enriched in heavy carbon isotope relative to a peatland gas since CO_2 is consumed during CO_2 reduction methanogenesis. In contrast, the second source produces ^{13}C-depleted (down to –98‰, Figure 5b) methane with relatively low concentrations (down to 2%, Figure 5a) predominantly via acetate fermentation. However, numerous studies showed that methane produced via acetate fermentation is more $\delta^{13}C$-enriched relative to methane produced via CO_2 reduction (Conrad, 2005; Hornibrook, 2009; Whiticar, 1999). What could resolve the discrepancy between the observed dominant role of acetate fermentation in production of CH_4 with relatively low concentrations and the pronounced depletion in ^{13}C of this methane?

We propose that chemolithotrophic acetogenesis followed by acetate fermentation methanogenesis (Conrad, 2020; Conrad et al., 2014; Dolfing, 1988) may be a likely mechanism explaining the observed pattern:

$$4H_2 + 2CO_2 \rightarrow CH_3COOH + 2H_2O$$

$$CH_3COOH \rightarrow CH_4 + CO_2$$
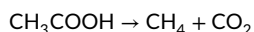
This mechanism can explain the abrupt decrease in DOC concentration from hundreds of mg L^{-1} in West Siberian raised bogs (Blanchet et al., 2017; Payandi-Rolland et al., 2020; Ratcliffe et al., 2017) to 7.7 ± 2.3 mg L^{-1} (average±std) in the seep water. As DOC in raised bogs typically has high aromatic content (Olefeldt & Roulet, 2012; Tfaily et al., 2013), its anaerobic degradation results in substantial H_2 production (Conrad, 2020; Kotsyurbenko et al., 2004). In the Quaternary and Oligocene aquifers of the West Siberian boreal zone, both concentrations of the alternative electron acceptors (Oshkin et al., 2014) and temperatures (0–6°C according to Bulatov, 2007) are low. At these conditions acetogens effectively

compete with Fe(III) reducers, sulfate reducers and methanogens for H_2 in cold lake sediments, tundra wetlands, and deep subterranean groundwater (see Drake et al., 2013 and references therein).

The first argument in favor of the proposed mechanism is a successful prediction of observed $\delta^{13}C(CH_4)$ in seep samples with methane concentrations less than 10%. The expected range of $\delta^{13}C(CH_4)$ in methane produced exclusively via this mechanism is –91‰ to –106‰. It is calculated as a sum of enrichment factors (–58‰ (Blaser et al., 2013; Conrad et al., 2014) and –10‰ – –25‰ (Conrad, 2005; Conrad & Klose, 2011; Whiticar, 1999) for the first and the second reactions, respectively) and median of $\delta^{13}C(CO_2)$ in seep gas. Mass balance calculation using relative contributions of this mechanism and CO_2 reduction (71% and 29%, respectively) and their isotopic compositions (–91‰ to –106‰ and –70‰, respectively) results in an expected range of $\delta^{13}C(CH_4)$ from –85‰ to –96‰. This is close to the observed range in seep samples with methane concentrations less than 10% (from –73‰ to –95‰, median –88‰). Furthermore, decrease in dissolved CO_2 concentration predicted by proposed mechanism (one molecule of CH_4 produced from one molecule of CO_2 via net reaction) is also corroborated by our data. In seeps with lower concentration of dissolved methane (presumably produced via acetate fermentation), concentrations of dissolved carbon dioxide were also significantly lower. The pH for these seeps was similar, suggesting that variable buffering by carbonates could not explain the lower CO_2 concentration in seep gas samples with methane concentration less than 10%.

4.4 | Assumptions and limitations

Our approach to calculating pathway contributions has several limitations, which could potentially bias our conclusions. We assumed no exchange of hydrogen isotopes between CH_4 and water. Such an exchange is unlikely to occur in the groundwater temperatures and Holocene timescale present in the Western Siberian boreal zone (Turner et al., 2022). We also assumed that there are only two pathways of methane production in groundwater (CO_2 reduction and acetate fermentation), while methyl-based methanogenesis could also contribute to the organic matter degradation in various environments (Bueno de Mesquita et al., 2023; Conrad, 2020). Since no data are currently available on the hydrogen isotope fractionation of methyl-based methanogenesis in the literature (Bueno de Mesquita et al., 2023), we cannot predict how this process can affect our calculations. However, while methyl-based methanogenesis is of primary importance in saline environments and animal guts, its contribution to the total methane production in freshwater environments seems to be minor (Bueno de Mesquita et al., 2023; Conrad, 2020). Another possible source of error is the assumption that regression models from Douglas et al. (2021) and Waldron et al. (1999) exclusively represent acetate fermentation. However, the contribution of CO_2 reduction or the influence of methane oxidation on these models would result in the underestimation of acetate fermentation role because both these process increase $\delta D(CH_4)$ relative to the

acetate fermentation. Finally, we assumed that there is a direct relationship through methanogenesis between seep δD(CH$_4$) and δD in co-occurring water, that is, there is no admixtures of allochthonous water or CH$_4$. To ensure this we exclude from analysis those gas samples, which were taken from seeps submerged by river water.

5 | CONCLUSION

This study aimed to examine the origin, metabolic pathways, and migration of methane in recently discovered terrestrial seeps located on the floodplains of the Ob and Irtysh Rivers in the middle of the West Siberia Lowlands. We found negligible concentration of hydrocarbons with more than one carbon atom in the seep gas, and values of δ^{13}C(CH$_4$), δD(CH$_4$) typical for methane of microbial origin. The radiocarbon age of seep methane ranged from 4.2 to 8.0 thousand years before present, pointing to Holocene-aged sources from peatlands. The close similarities between seep and peatland gas suggest that methane is migrating from raised bogs (the source) to seeps located within the floodplains of the West Siberia rivers (hot spots of its release to the atmosphere) through groundwater. These processes operate at a regional spatial and Holocene temporal scale.

The stable isotope compositions of the seep methane indicate the absence of significant oxidation during transport from bogs to seeps as well as continual mixing of methane produced in two different biogeochemical settings. While methane with the highest concentrations is likely produced in situ in raised bogs via CO$_2$ reduction, methane with relatively low concentrations could be produced in groundwater from DOC, which migrates from raised bogs. Discrepancy between the strong δ^{13}C depletion and the high contribution of acetate fermentation for methane with relatively low concentrations could be explained by the biogeochemical mechanism, which couples acetogenesis and acetate fermentation methanogenesis.

These findings reveal the close links between peatlands, groundwater, and river floodplains in the West Siberia Lowlands in terms of methane-migration pathways from terrestrial to aquatic ecosystems and its eventual large emissions to the atmosphere. Since the groundwater substantially contributes to the river flow in the non-permafrost part of the West Siberia Lowlands (Frey et al., 2007), it could transport methane not only to seeps but also to rivers and streams, thereby increasing methane emission from them. This *groundwater pathway* in the terrestrial methane cycle may be overlooked in other regions where raised bogs are widely present. Further research is needed to understand the environmental controls of methane concentration in seep water on different spatial and temporal scales, to estimate the contribution of West Siberia boreal zone seeps to the global methane budget, and to investigate the biogeochemistry of carbon transformation in West Siberia aquifers.

AUTHOR CONTRIBUTIONS
Conceptualization: Aleksandr F. Sabrekov, Irina E. Terentieva. *Data curation, formal analysis, and funding acquisition*: Aleksandr F. Sabrekov. *Investigation*: Aleksandr F. Sabrekov, Irina E. Terentieva, Yuriy V. Litti, Ekaterina V. Parkhomchuk, Alexey V. Petrozhitskiy. *Methodology*: Aleksandr F. Sabrekov, Irina E. Terentieva, Yuriy V. Litti. *Validation*: Aleksandr F. Sabrekov, Yuriy V. Litti. *Resources*: Aleksandr F. Sabrekov, Irina E. Terentieva, Yuriy V. Litti, Peter N. Kalinkin, Dmitry V. Kuleshov. *Writing—original draft preparation*: Aleksandr F. Sabrekov. *Writing—review and editing*: Aleksandr F. Sabrekov, Irina E. Terentieva, Gregory J. McDermid, Anatoly S. Prokushkin, Mikhail V. Glagolev. *Visualization*: Aleksandr F. Sabrekov, Irina E. Terentieva. *Project administration*: Aleksandr F. Sabrekov, Irina E. Terentieva. All authors have read and agreed to the published version of the manuscript.

CONFLICT OF INTEREST STATEMENT
The authors declare that they have no conflicts of interest.

DATA AVAILABILITY STATEMENT
The data that support the findings of this study are openly available in Dryad at https://doi.org/10.5061/dryad.31zcrjdr4.

ORCID
Aleksandr F. Sabrekov https://orcid.org/0000-0002-6501-912X
Irina E. Terentieva https://orcid.org/0000-0002-7798-0815
Gregory J. McDermid https://orcid.org/0000-0001-8079-3730
Yuriy V. Litti https://orcid.org/0000-0002-5457-4603
Anatoly S. Prokushkin https://orcid.org/0000-0001-8721-2142
Mikhail V. Glagolev https://orcid.org/0000-0002-4327-1885
Alexey V. Petrozhitskiy https://orcid.org/0000-0002-6653-2232
Peter N. Kalinkin https://orcid.org/0000-0003-1030-9100
Dmitry V. Kuleshov https://orcid.org/0000-0002-3897-0817
Ekaterina V. Parkhomchuk https://orcid.org/0000-0003-2200-884X

REFERENCES
Alekseychik, P., Mammarella, I., Karpov, D., Dengel, S., Terentieva, I., Sabrekov, A., Glagolev, M., & Lapshina, E. (2017). Net ecosystem exchange and energy fluxes measured with the eddy covariance technique in a Western Siberian bog. *Atmospheric*

Chemistry and Physics, 17, 9333–9345. https://doi.org/10.5194/acp-17-9333-2017

Aravena, R., Warner, B. G., Charman, D. J., Belyea, L. R., Mathur, S. P., & Dinel, H. (1993). Carbon isotopic composition of deep carbon gases in an ombrogenous peatland, northwestern Ontario, Canada. *Radiocarbon*, 35(2), 271–276. https://doi.org/10.1017/S0033822200064948

Aravena, R., Wassenaar, L. I., & Spiker, E. C. (2004). Chemical and carbon isotopic composition of dissolved organic carbon in a regional confined methanogenic aquifer. *Isotopes in Environmental and Health Studies*, 40(2), 103–114. https://doi.org/10.1080/10256010410001671050

Beer, J., & Blodau, C. (2007). Transport and thermodynamics constrain belowground carbon turnover in a northern peatland. *Geochimica et Cosmochimica Acta*, 71(12), 2989–3002. https://doi.org/10.1016/j.gca.2007.03.010

Belova, S. E., Oshkin, I. Y., Glagolev, M. V., Lapshina, E. D., Maksyutov, S., & Dedysh, S. N. (2013). Methanotrophic bacteria in cold seeps of the floodplains of northern rivers. *Microbiology*, 82(6), 743–750. https://doi.org/10.1134/S0026261713060040

Bergamaschi, P. (1997). Seasonal variations of stable hydrogen and carbon isotope ratios in methane from a Chinese rice paddy. *Journal of Geophysical Research: Atmospheres*, 102(D21), 25383–25393. https://doi.org/10.1029/97JD01664

Blanchet, G., Guillet, S., Calliari, B., Corona, C., Edvardsson, J., Stoffel, M., & Bragazza, L. (2017). Impacts of regional climatic fluctuations on radial growth of Siberian and scots pine at Mukhrino mire (Central-Western Siberia). *Science of the Total Environment*, 574, 1209–1216. https://doi.org/10.1016/j.scitotenv.2016.06.225

Blaser, M. B., Dreisbach, L. K., & Conrad, R. (2013). Carbon isotope fractionation of 11 acetogenic strains grown on H_2 and CO_2. *Applied and Environmental Microbiology*, 79, 1787–1794. https://doi.org/10.1128/AEM.03203-12

Bronk Ramsey, C. (2009). Bayesian analysis of radiocarbon dates. *Radiocarbon*, 51, 337–360. https://doi.org/10.1017/S0033822200033865

Brown, J., Ferrians, O. J., Jr., Heginbottom, J. A., & Melnikov, E. S. (Eds.). (1997). *Circum-Arctic map of permafrost and ground-ice conditions, Circum-Pac. Map Ser. CP-45, 1 sheet, scale 1:10,000,000*. USGS. https://doi.org/10.3133/cp45

Bueno de Mesquita, C. P., Wu, D., & Tringe, S. G. (2023). Methyl-based methanogenesis: An ecological and genomic review. *Microbiology and Molecular Biology Reviews*, 87(1), e00024–e00022. https://doi.org/10.1128/mmbr.00024-22

Bulatov, V. I. (2007). *Geography and ecology of Khanty-Mansiysk and its natural surroundings*. Informatsionno-Izdatel'skiy Tsentr In Russian.

Canadell, J. G., Monteiro, P. M. S., Costa, M. H., Cotrim da Cunha, L., Cox, P. M., Eliseev, A. V., Henson, S., Ishii, M., Jaccard, S., Koven, C., Lohila, A., Patra, P. K., Piao, S., Rogelj, J., Syampungani, S., Zaehle, S., & Zickfeld, K. (2021). Global carbon and other biogeochemical cycles and feedbacks. In V. Masson-Delmotte, P. Zhai, A. Pirani, S. L. Connors, C. Péan, S. Berger, N. Caud, Y. Chen, L. Goldfarb, M. I. Gomis, M. Huang, K. Leitzell, E. Lonnoy, J. B. R. Matthews, T. K. Maycock, T. Waterfield, O. Yelekçi, R. Yu, & B. Zhou (Eds.), *Climate change 2021: The physical science basis. Contribution of Working Group I to the Sixth Assessment Report of the Intergovernmental Panel on Climate Change* (pp. 673–816). Cambridge University Press. https://doi.org/10.1017/9781009157896.007

Chanton, J. P., Bauer, J. E., Glaser, P. A., Siegel, D. I., Kelley, C. A., Tyler, S. C., Romanowicz, E. H., & Lazrus, A. (1995). Radiocarbon evidence for the substrates supporting methane formation within northern Minnesota peatlands. *Geochimica et Cosmochimica Acta*, 59(17), 3663–3668. https://doi.org/10.1016/0016-7037(95)00240-Z

Ciotoli, G., Procesi, M., Etiope, G., Fracassi, U., & Ventura, G. (2020). Influence of tectonics on global scale distribution of geological methane emissions. *Nature Communications*, 11(1), 1–8. https://doi.org/10.1038/s41467-020-16229-1

Clark, I. D., & Fritz, P. (2013). *Environmental isotopes in hydrogeology, 3rd ed.* CRC Press.

Clymo, R. S., & Bryant, C. L. (2008). Diffusion and mass flow of dissolved carbon dioxide, methane, and dissolved organic carbon in a 7-m deep raised peat bog. *Geochimica et Cosmochimica Acta*, 72(8), 2048–2066. https://doi.org/10.1016/j.gca.2008.01.032

Conrad, R. (2005). Quantification of methanogenic pathways using stable carbon isotopic signatures: A review and a proposal. *Organic Geochemistry*, 36(5), 739–752. https://doi.org/10.1016/j.orggeochem.2004.09.006

Conrad, R. (2020). Importance of hydrogenotrophic, aceticlastic and methylotrophic methanogenesis for methane production in terrestrial, aquatic and other anoxic environments: A mini review. *Pedosphere*, 30(1), 25–39. https://doi.org/10.1016/S1002-0160(18)60052-9

Conrad, R., Claus, P., Chidthaisong, A., Lu, Y., Scavino, A. F., Liu, Y., Angel, R., Galand, P. E., Casper, P., Guerin, F., & Enrich-Prast, A. (2014). Stable carbon isotope biogeochemistry of propionate and acetate in methanogenic soils and lake sediments. *Organic Geochemistry*, 73, 1–7. https://doi.org/10.1016/j.orggeochem.2014.03.010

Conrad, R., & Klose, M. (2011). Stable carbon isotope discrimination in rice field soil during acetate turnover by syntrophic acetate oxidation or acetoclastic methanogenesis. *Geochimica et Cosmochimica Acta*, 75(6), 1531–1539. https://doi.org/10.1016/j.gca.2010.12.019

Cook, P. (2020). *Introduction to isotopes and environmental tracers as indicators of groundwater flow*. Groundwater Project.

Corbett, J. E., Tfaily, M. M., Burdige, D. J., Glaser, P. H., & Chanton, J. P. (2015). The relative importance of methanogenesis in the decomposition of organic matter in northern peatlands. *Journal of Geophysical Research: Biogeosciences*, 120(2), 280–293. https://doi.org/10.1002/2014JG002797

Dolfing, J. (1988). Acetogenesis. In A. J. B. Zehnder (Ed.), *Biology of anaerobic microorganisms* (pp. 417–468). Wiley.

Danilova, O. V., Ivanova, A. A., Terent'eva, I. E., Glagolev, M. V., & Sabrekov, A. F. (2021). Microbial community composition of floodplains shallow-water seeps in the Bolshaya Rechka floodplain, Western Siberia. *Microbiology*, 90(5), 632–642. https://doi.org/10.1134/S0026261721050040

Douglas, P. M., Stratigopoulos, E., Park, S., & Phan, D. (2021). Geographic variability in freshwater methane hydrogen isotope ratios and its implications for global isotopic source signatures. *Biogeosciences*, 18(11), 3505–3527. https://doi.org/10.5194/bg-18-3505-2021

Drake, H. L., Küsel, K., & Matthies, C. (2013). Acetogenic prokaryotes. In E. Rosenberg, E. F. DeLong, S. Lory, E. Stackebrandt, & F. Thompson (Eds.), *The prokaryotes: Prokaryotic physiology and biochemistry* (pp. 3–60). Springer. https://doi.org/10.1007/978-3-642-30141-4_61

Dubinina, E. O., Miroshnikov, A. Y., Kossova, S. A., & Shchuka, S. A. (2019). Modification of the Laptev Sea freshened shelf waters based on isotope and salinity relations. *Geochemistry International*, 57(1), 1–19. https://doi.org/10.1134/S001670291901004X

Dyukarev, E., Filippova, N., Karpov, D., Shnyrev, N., Zarov, E., Filippov, I., Voropay, N., Avilov, V., Artamonov, A., & Lapshina, E. (2021). Hydrometeorological dataset of west Siberian boreal peatland: A 10-year record from the Mukhrino field station. *Earth System Science Data*, 13(6), 2595–2605. https://doi.org/10.5194/essd-13-2595-2021

Etiope, G. (2015). *Natural gas seepage*. Springer.

Etiope, G., Ciotoli, G., Schwietzke, S., & Schoell, M. (2019). Gridded maps of geological methane emissions and their isotopic signature. *Earth System Science Data*, 11(1), 1–22. https://doi.org/10.5194/essd-11-1-2019

Forster, P., Storelvmo, T., Armour, K., Collins, W., Dufresne, J.-L., Frame, D., Lunt, D. J., Mauritsen, T., Palmer, M. D., Watanabe, M., Wild, M.,

& Zhang, H. (2021). The Earth's energy budget, climate feedbacks, and climate sensitivity. In V. Masson-Delmotte, P. Zhai, A. Pirani, S. L. Connors, C. Péan, S. Berger, N. Caud, Y. Chen, L. Goldfarb, M. I. Gomis, M. Huang, K. Leitzell, E. Lonnoy, J. B. R. Matthews, T. K. Maycock, T. Waterfield, O. Yelekçi, R. Yu, & B. Zhou (Eds.), *Climate change 2021: The physical science basis. Contribution of Working Group I to the Sixth Assessment Report of the Intergovernmental Panel on Climate Change* (pp. 923–1054). Cambridge University Press. https://doi.org/10.1017/9781009157896.009

Fraser, C. J. D., Roulet, N. T., & Lafleur, M. (2001). Groundwater flow patterns in a large peatland. *Journal of Hydrology*, 246(1–4), 142–154. https://doi.org/10.1016/S0022-1694(01)00362-6

Frey, K. E., Siegel, D. I., & Smith, L. C. (2007). Geochemistry of west Siberian streams and their potential response to permafrost degradation. *Water Resources Research*, 43(3), W03406. https://doi.org/10.1029/2006WR004902

Glaser, P. H., Siegel, D. I., Chanton, J. P., Reeve, A. S., Rosenberry, D. O., Corbett, J. E., Dasgupta, S., & Levy, Z. (2016). Climatic drivers for multidecadal shifts in solute transport and methane production zones within a large peat basin. *Global Biogeochemical Cycles*, 30(11), 1578–1598. https://doi.org/10.1002/2016GB005397

Golding, S. D., Boreham, C. J., & Esterle, J. S. (2013). Stable isotope geochemistry of coal bed and shale gas and related production waters: A review. *International Journal of Coal Geology*, 120, 24–40. https://doi.org/10.1016/j.coal.2013.09.001

Goncharov, I. V., Korobochkina, V. G., Oblasov, N. V., & Samoilenko, V. V. (2005). Nature of hydrocarbon gases in the southeast of Western Siberia. *Geochemistry International*, 43, 810–815.

Gröning, M., & Rozanski, K. (2003). Uncertainty assessment of environmental tritium measurements in water. *Accreditation for Quality Assurance*, 8, 359–366. https://doi.org/10.1007/s00769-003-0631-y

Hope, D., Dawson, J. J., Cresser, M. S., & Billett, M. F. (1995). A method for measuring free CO_2 in upland streamwater using headspace analysis. *Journal of Hydrology*, 166(1–2), 1–14. https://doi.org/10.1016/0022-1694(94)02628-O

Hornibrook, E. R. (2009). The stable carbon isotope composition of methane produced and emitted from northern peatlands. In A. J. Baird, L. R. Belyea, X. Comas, A. S. Reeve, & L. D. Slater (Eds.), *Carbon cycling in northern peatlands (Geophysical Monograph Series)* (Vol. 184, pp. 187–203). American Geophysical Union. https://doi.org/10.1029/2008GM000828

Hornibrook, E. R., Longstaffe, F. J., & Fyfe, W. S. (1997). Spatial distribution of microbial methane production pathways in temperate zone wetland soils: Stable carbon and hydrogen isotope evidence. *Geochimica et Cosmochimica Acta*, 61(4), 745–753. https://doi.org/10.1016/S0016-7037(96)00368-7

International Atomic Energy Agency. (2022). *Global network of isotopes in precipitation*. The GNIP Database https://nucleus.iaea.org/wiser

Jacops, E., Volckaert, G., Maes, N., Weetjens, E., & Govaerts, J. (2013). Determination of gas diffusion coefficients in saturated porous media: He and CH_4 diffusion in boom clay. *Applied Clay Science*, 83, 217–223. https://doi.org/10.1016/j.clay.2013.08.047

Jasechko, S. (2019). Global isotope hydrogeology—review. *Reviews of Geophysics*, 57(3), 835–965. https://doi.org/10.1029/2018RG000627

Jean-Baptiste, P., Fourré, E., Gaubi, E., Minster, B., Aquilina, L., Labasque, T., Michelot, J. L., Massault, M., & Mammou, A. B. (2017). Underground renewal time and mixing of the main mineral waters of Tunisia: A multi-tracer study. *Applied Geochemistry*, 85, 10–18. https://doi.org/10.1016/j.apgeochem.2017.08.006

Khafizov, S., Syngaevsky, P., & Dolson, J. C. (2022). The west Siberian Super Basin: The largest and most prolific hydrocarbon basin in the world. *AAPG Bulletin*, 106(3), 517–572. https://doi.org/10.1306/11192121086

Kinnaman, F. S., Valentine, D. L., & Tyler, S. C. (2007). Carbon and hydrogen isotope fractionation associated with the aerobic microbial oxidation of methane, ethane, propane and butane. *Geochimica et Cosmochimica Acta*, 71(2), 271–283. https://doi.org/10.1016/j.gca.2006.09.007

Kosykh, N. P., Mironycheva-Tokareva, N. P., Peregon, A. M., & Parshina, E. K. (2008). Biological productivity of bogs in the middle taiga subzone of Western Siberia. *Russian Journal of Ecology*, 39, 466–474. https://doi.org/10.1134/S1067413608070023

Kotsyurbenko, O. R., Chin, K. J., Glagolev, M. V., Stubner, S., Simankova, M. V., Nozhevnikova, A. N., & Conrad, R. (2004). Acetoclastic and hydrogenotrophic methane production and methanogenic populations in an acidic west-Siberian peat bog. *Environmental Microbiology*, 6(11), 1159–1173. https://doi.org/10.1111/j.1462-2920.2004.00634.x

Kraev, G., Rivkina, E., Vishnivetskaya, T., Belonosov, A., van Huissteden, J., Kholodov, A., Smirnov, A., Kudryavtsev, A., Teshebaeva, K., & Zamolodchikov, D. (2019). Methane in gas shows from boreholes in epigenetic permafrost of Siberian Arctic. *Geosciences*, 9, 67. https://doi.org/10.3390/geosciences9020067

Kraev, G., Schulze, E.-D., Yurova, A., Kholodov, A., Chuvilin, E., & Rivkina, E. (2017). Cryogenic displacement and accumulation of biogenic methane in frozen soils. *Atmosphere*, 8, 105. https://doi.org/10.3390/atmos8060105

Kremenetski, K. V., Velichko, A. A., Borisova, O. K., MacDonald, G. M., Smith, L. C., Frey, K. E., & Orlova, L. A. (2003). Peatlands of the Western Siberian lowlands: Current knowledge on zonation, carbon content and late quaternary history. *Quaternary Science Reviews*, 22(5–7), 703–723. https://doi.org/10.1016/S0277-3791(02)00196-8

Laanbroek, H. J. (2010). Methane emission from natural wetlands: Interplay between emergent macrophytes and soil microbial processes. A mini-review. *Annals of Botany*, 105(1), 141–153. https://doi.org/10.1093/aob/mcp201

Lehner, B., & Döll, P. (2004). Development and validation of a global database of lakes, reservoirs and wetlands. *Journal of Hydrology*, 296(1–4), 1–22. https://doi.org/10.1016/j.jhydrol.2004.03.028

Leschinsky, S. V., Maschenko, E. N., Orlova, L. A., Burkanova, E. M., Konovalova, V. A., Teterina, I. I., & Gevlia, K. M. (2006). Multidisciplinary paleontological and stratigraphic studies at Lugovskoe site (2002–2004). *Archeology, Ethnography and Anthropology of Eurasia*, 25(1), 54–69 (In Russian).

Levy, Z. F., Siegel, D. I., Dasgupta, S. S., Glaser, P. H., & Welker, J. M. (2014). Stable isotopes of water show deep seasonal recharge in northern bogs and fens. *Hydrological Processes*, 28, 4938–4952. https://doi.org/10.1002/hyp.9983

Lokshina, L., Vavilin, V., Litti, Y., Glagolev, M., Sabrekov, A., Kotsyurbenko, O., & Kozlova, M. (2019). Methane production in a west Siberian eutrophic fen is much higher than carbon dioxide production: Incubation of peat samples, stoichiometry, stable isotope dynamics, modeling. *Water Resources*, 46(1), S110–S125. https://doi.org/10.1134/S0097807819070133

Lysikov, A. I., Kalinkin, P. N., Sashkina, K. A., Okunev, A. G., Parkhomchuk, E. V., Rastigeev, S. A., Parkhomchuk, V. V., Kuleshov, D. V., Vorobyeva, E. E., & Dralyuk, R. I. (2018). Novel simplified absorption-catalytic method of sample preparation for AMS analysis designed at the Laboratory of Radiocarbon Methods of analysis (LRMA) in Novosibirsk Akademgorodok. *International Journal of Mass-Spectrometry*, 433, 11–18. https://doi.org/10.1016/j.ijms.2018.08.003

Masing, V., Botch, M., & Läänelaid, A. (2010). Mires of the former Soviet Union. *Wetlands Ecology and Management*, 18(4), 397–433. https://doi.org/10.1007/s11273-008-9130-6

McNair, H. M., Miller, J. M., & Snow, N. H. (2019). *Basic gas chromatography*. John Wiley & Sons.

Milkov, A. V. (2010). Methanogenic biodegradation of petroleum in the west Siberian Basin (Russia): Significance for formation of giant Cenomanian gas pools. *AAPG Bulletin*, 94(10), 1485–1541. https://doi.org/10.1306/01051009122

Milkov, A. V. (2018). Secondary microbial gas. In H. Wilkes (Ed.), *Hydrocarbons, oils and lipids: Diversity, origin, chemistry and fate. Handbook of hydrocarbon and lipid microbiology* (pp. 613–622). Springer. https://doi.org/10.1007/978-3-319-54529-5_22-1

Milkov, A. V., & Etiope, G. (2018). Revised genetic diagrams for natural gases based on a global dataset of >20,000 samples. *Organic Geochemistry*, *125*, 109–120. https://doi.org/10.1016/j.orggeochem.2018.09.002

Morgenstern, U., & Taylor, C. B. (2009). Ultra low-level tritium measurement using electrolytic enrichment and LSC. *Isotopes in Environmental and Health Studies*, *45*, 96–117. https://doi.org/10.1080/10256010902931194

Obu, J., Westermann, S., Kääb, A., & Bartsch, A. (2018). *Ground Temperature Map, 2000–2016, Northern Hemisphere Permafrost*. Alfred Wegener Institute, Helmholtz Centre for Polar and Marine Research, Bremerhaven, Pangaea. https://doi.org/10.1594/PANGAEA.888600

Olefeldt, D., & Roulet, N. T. (2012). Effects of permafrost and hydrology on the composition and transport of dissolved organic carbon in a subarctic peatland complex. *Journal of Geophysical Research*, *117*, G01005. https://doi.org/10.1029/2011JG001819

Oremland, R. S., Whiticar, M. J., Strohmaier, F. E., & Kiene, R. P. (1988). Bacterial ethane formation from reduced, ethylated sulphur compounds in anoxic sediments. *Geochimica et Cosmochimica Acta*, *52*, 1895–1904. https://doi.org/10.1016/0016-7037(88)90013-0

Oshkin, I. Y., Wegner, C.-E., Lüke, C., Glagolev, M. V., Filippov, I. V., Pimenov, N. V., Liesack, W., & Dedysh, S. N. (2014). Gammaproteobacterial methanotrophs dominate cold methane seeps in floodplains of west Siberian rivers. *Applied and Environmental Microbiology*, *80*(19), 5944–5954. https://doi.org/10.1128/AEM.01539-14

Parkhomchuk, V. V., & Rastigeev, S. A. (2011). Accelerator mass spectrometer of the center for collective use of the Siberian Branch of the Russian Academy of Sciences. *Journal of Surface Investigation*, *5*(6), 1068–1072. https://doi.org/10.1134/S1027451011110140

Payandi-Rolland, D., Shirokova, L. S., Tesfa, M., Benezeth, P., Lim, A. G., Kuzmina, D., Karlsson, J., Giesler, R., & Pokrovsky, O. S. (2020). Dissolved organic matter biodegradation along a hydrological continuum in permafrost peatlands. *Science of the Total Environment*, *749*, 141463. https://doi.org/10.1016/j.scitotenv.2020.141463

Pekel, J.-F., Cottam, A., Gorelick, N., & Belward, A. S. (2016). High-resolution mapping of global surface water and its long-term changes. *Nature*, *540*, 418–422. https://doi.org/10.1038/nature20584

Rasigraf, O., Vogt, C., Richnow, H. H., Jetten, M. S., & Ettwig, K. F. (2012). Carbon and hydrogen isotope fractionation during nitrite-dependent anaerobic methane oxidation by *Methylomirabilis oxyfera*. *Geochimica et Cosmochimica Acta*, *89*, 256–264. https://doi.org/10.1016/j.gca.2012.04.054

Ratcliffe, J. L., Creevy, A., Andersen, R., Zarov, E., Gaffney, P. P., Taggart, M. A., Mazei, Y., Tsyganov, A. N., Rowson, J. G., Lapshina, E. D., & Payne, R. J. (2017). Ecological and environmental transition across the forested-to-open bog ecotone in a west Siberian peatland. *Science of the Total Environment*, *607*, 816–828. https://doi.org/10.1016/j.scitotenv.2017.06.276

Reeve, A. S., Siegel, D. I., & Glaser, P. H. (2000). Simulating vertical flow in large peatlands. *Journal of Hydrology*, *227*(1–4), 207–217. https://doi.org/10.1016/S0022-1694(99)00183-3

Reeve, A. S., Tyczka, Z. D., Comas, X., & Slater, L. D. (2009). The influence of permeable mineral lenses on peatland hydrology. In A. L. Baird, L. R. Belyea, X. Comas, A. S. Reeve, & L. D. Slater (Eds.), *Northern peatlands and carbon cycling (Geophysical Monograph Series)* (Vol. *184*, pp. 289–297). American Geophysical Union. https://doi.org/10.1029/2008GM000825

Reimer, P. J., Austin, W. E. N., Bard, E., Bayliss, A., Blackwell, P. G., Bronk Ramsey, C., Butzin, M., Cheng, H., Edwards, R. L., Friedrich, M., Grootes, P. M., Guilderson, T. P., Hajdas, I., Heaton, T. J., Hogg, A. G., Hughen, K. A., Kromer, B., Manning, S. W., Muscheler, R., … Talamo, S. (2020). The IntCal20 northern hemisphere radiocarbon age calibration curve (0–55 kBP). *Radiocarbon*, *62*(4), 725–757. https://doi.org/10.1017/RDC.2020.41

Rivkina, E., Shcherbakova, V., Laurinavichius, K., Petrovskaya, L., Krivushin, K., Kraev, G., Pecheritsina, S., & Gilichinsky, D. (2007). Biogeochemistry of methane and methanogenic *archaea* in permafrost. *FEMS Microbiology Ecology*, *61*(1), 1–15. https://doi.org/10.1111/j.1574-6941.2007.00315.x

Sabrekov, A. F., Danilova, O. V., Terentieva, I. E., Ivanova, A. A., Belova, S. E., Litti, Y. V., Glagolev, M. V., & Dedysh, S. N. (2021). Atmospheric methane consumption and methanotroph communities in west Siberian boreal upland Forest ecosystems. *Forests*, *12*, 1738. https://doi.org/10.3390/f12121738

Sander, R. (2015). Compilation of Henry's law constants (version 4.0) for water as solvent. *Atmospheric Chemistry and Physics*, *15*, 4399–4981. https://doi.org/10.5194/acp-15-4399-2015

Saunois, M., Stavert, A. R., Poulter, B., Bousquet, P., Canadell, J. G., Jackson, R. B., Raymond, P. A., Dlugokencky, E. J., Houweling, S., Patra, P. K., Ciais, P., Arora, V. K., Bastviken, D., Bergamaschi, P., Blake, D. R., Brailsford, G., Bruhwiler, L., Carlson, K. M., Carrol, M., … Zhuang, Q. (2020). The global methane budget 2000–2017. *Earth System Science Data*, *12*, 1561–1623. https://doi.org/10.5194/essd-12-1561-2020

Schumacher, D. (2010). Integrating hydrocarbon microseepage data with seismic data doubles exploration success. In *Proceedings thirty-fourth annual conference and exhibition (May 2010, IPA10-G-104)*. Indonesian Petroleum Association. https://doi.org/10.29118/IPA.1277.10.G.104

Sheng, Y., Smith, L. C., MacDonald, G. M., Kremenetski, K. V., Frey, K. E., Velichko, A. A., Lee, M., Beilman, D. W., & Dubinin, P. (2004). A high-resolution GIS-based inventory of the west Siberian peat carbon pool. *Global Biogeochemical Cycles*, *18*(3), GB3004. https://doi.org/10.1029/2003GB002190

Shimada, M., Itoh, T., Motooka, T., Watanabe, M., Shiraishi, T., Thapa, R., & Lucas, R. (2014). New global forest/non-forest maps from ALOS PALSAR data (2007–2010). *Remote Sensing of Environment*, *155*, 13–31. https://doi.org/10.1016/j.rse.2014.04.014

Shoemaker, J. K., & Schrag, D. P. (2010). Subsurface characterization of methane production and oxidation from a New Hampshire wetland. *Geobiology*, *8*(3), 234–243. https://doi.org/10.1111/j.1472-4669.2010.00239.x

Terentieva, I., Filippov, I., Sabrekov, A., & Glagolev, M. (2022). Mapping onshore CH_4 seeps in Western Siberian floodplains using convolutional neural network. *Remote Sensing*, *14*(11), 2661. https://doi.org/10.3390/rs14112661

Terentieva, I. E., Glagolev, M. V., Lapshina, E. D., Sabrekov, A. F., & Maksyutov, S. (2016). Mapping of west Siberian taiga wetland complexes using Landsat imagery: Implications for methane emissions. *Biogeosciences*, *13*, 4615–4626. https://doi.org/10.5194/bg-13-4615-2016

Tfaily, M. M., Hamdan, R., Corbett, J. E., Chanton, J. P., Glaser, P. H., & Cooper, W. T. (2013). Investigating dissolved organic matter decomposition in northern peatlands using complimentary analytical techniques. *Geochimica et Cosmochimica Acta*, *112*, 116–129. https://doi.org/10.1016/j.gca.2013.03.002

Turner, A. C., Pester, N. J., Bill, M., Conrad, M. E., Knauss, K. G., & Stolper, D. A. (2022). Experimental determination of hydrogen isotope exchange rates between methane and water under hydrothermal conditions. *Geochimica et Cosmochimica Acta*, *329*, 231–255. https://doi.org/10.1016/j.gca.2022.04.029

Turunen, J., Tahvanainen, T., Tolonen, K., & Pitkänen, A. (2001). Carbon accumulation in west Siberian mires, Russia sphagnum peatland distribution in North America and Eurasia during the past 21,000 years. *Global Biogeochemical Cycles*, *15*(2), 285–296. https://doi.org/10.1029/2000GB001312

Waldron, S., Lansdown, J., Scott, E., Fallick, A., & Hall, A. (1999). The global influence of the hydrogen isotope composition of water on

that of bacteriogenic methane from shallow freshwater environments. *Geochimica et Cosmochimica Acta, 63*, 2237–2245. https://doi.org/10.1016/S0016-7037(99)00192-1

Walter Anthony, K. M., Anthony, P., Grosse, G., & Chanton, J. (2012). Geologic methane seeps along boundaries of Arctic permafrost thaw and melting glaciers. *Nature Geoscience, 5*, 419–426. https://doi.org/10.1038/ngeo1480

Whiticar, M. J. (1999). Carbon and hydrogen isotope systematics of bacterial formation and oxidation of methane. *Chemical Geology, 161*(1–3), 291–314. https://doi.org/10.1016/S0009-2541(99)00092-3

Whiticar, M. J. (2020). The biogeochemical methane cycle. In H. Wilkes (Ed.), *Hydrocarbons, oils and lipids: Diversity, origin, chemistry and fate. Handbook of hydrocarbon and lipid microbiology* (pp. 669–746). Springer. https://doi.org/10.1007/978-3-319-54529-5_22-1

Xie, S., Lazar, C. S., Lin, Y. S., Teske, A., & Hinrichs, K. U. (2013). Ethane- and propane-producing potential and molecular characterization of an ethanogenic enrichment in an anoxic estuarine sediment. *Organic Geochemistry, 59*, 37–48. https://doi.org/10.1016/j.orggeochem.2013.03.001

Zarov, E. A., Lapshina, E. D., Kuhlmann, I., & Schulze, E.-D. (2021). Dissolved organic carbon vertical movement and carbon accumulation in west Siberian peatlands. *Biogeosciences Discussions*. https://doi.org/10.5194/bg-2021-211

SUPPORTING INFORMATION

Additional supporting information can be found online in the Supporting Information section at the end of this article.